THE ASTROPHYSICAL JOURNAL, 298:58–79, 1985 November 1

RELATIVISTIC STELLAR DYNAMICS ON THE COMPUTER. II. PHYSICAL APPLICATIONS

STUART L. SHAPIRO AND SAUL A. TEUKOLSKY
Center for Radiophysics and Space Research, and Departments of Astronomy and Physics, Cornell University
Received 1985 February 4; accepted 1985 April 24

ABSTRACT

This is the second of a series of papers on the numerical solution of Einstein's equations for the dynamical evolution of a *collisionless* gas of particles in general relativity. This paper deals mainly with applications to spherical star clusters. Previous studies were restricted to static equilibria and linear perturbations. We bring together the tools of numerical relativity and N-body particle simulation to follow the full nonlinear evolution of such dynamical systems.

We investigate the stability of equilibrium configurations. We present strong numerical evidence that, as in the case of fluid stars, the binding energy maximum along an equilibrium sequence does in fact signal the onset of dynamical instability. We explore the fate of unstable clusters, including those that collapse to black holes. We find that even in the case of extremely centrally condensed configurations with extensive Newtonian halos, an appreciable fraction of the *total* cluster mass collapses to a central black hole in a few dynamical times. This occurs because of the "avalanche effect" predicted by Zel'dovich and Podurets. The result may be important for the origin of quasars and active galactic nuclei via the collapse of dense star clusters to supermassive black holes.

We discuss the dynamical stability of Newtonian polytropic clusters and report numerical evidence confirming that all equilibrium polytropes (even those whose distribution function increases with energy) are stable.

We explore violent relaxation in the relativistic domain. A collisionless configuration can either achieve virial equilibrium via this mechanism or else collapse to a black hole. The outcome of such processes in the early universe may be relevant to the missing mass and dark matter problems.

Subject headings: clusters: globular — numerical methods — relativity — stars: stellar dynamics

I. INTRODUCTION

As described in Paper I of this series (Shapiro and Teukolsky 1985*a*), it is now possible to solve Einstein's equations for the dynamical evolution of a *collisionless* gas of particles numerically, at least for spherical systems. Given the initial positions and velocities of a large number of self-gravitating, but otherwise noninteracting, particles, we can determine the gravitational field and matter distribution at subsequent times. The particle velocities can approach the speed of light, and the gravitational field can become arbitrarily strong, even resulting in black hole formation. The computational method joins together the techniques of numerical relativity with those of N-body particle simulations. Paper I provides some historical background to this problem, followed by a detailed presentation of the computational method and a series of test-bed calculations to assess the reliability of the code.

The purpose of this paper is to apply the code to address several outstanding theoretical issues in relativistic stellar dynamics. This is a subject that was extremely active in the period 1965–70, with impetus coming from attempts to construct quasar models. Although much progress was made in understanding the behavior of star clusters in the relativistic domain, many important questions could not be answered. One such question concerns the stability and dynamical fate of relativistic star clusters. The perturbation equations for an equilibrium cluster can be cast in the form of a variational principle (Ipser and Thorne 1968; Ipser 1969). Using suitable trial functions, one can locate the point along an equilibrium sequence where the oscillation frequency ω^2 becomes negative. This is a sufficient criterion for instability. By analogy with equilibrium sequences of fluid stars, one can also study the fractional binding energy of an equilibrium cluster sequence. In several cases, the maximum fractional binding energy was found to coincide with the point where ω^2 became negative, to within numerical accuracy. This led to the conjecture that the location of the first maximum in the binding energy of a suitably parametrized sequence signals the onset of instability. However, it has only been proved that the conjecture is a sufficient condition for stability; in other words, members of an appropriate equilibrium sequence are stable at least up to the first maximum in the binding energy (Ipser 1980). Moreover, there are cases where the binding energy criterion and the best trial function determination of the onset of instability are well separated. Is this because the binding energy criterion is not, in fact, necessary and sufficient, or is it because the trial function approach is inaccurate? We address this issue in § II.

What is the ultimate fate of an equilibrium star cluster that is unstable? We might expect that a fairly homogeneous cluster might collapse homologously, perhaps all the way to a black hole. On the other hand, if the initial cluster is very centrally condensed with a pronounced core-halo structure, then we might expect only a small portion of the core to collapse to a black hole. We shall show that this expectation is in fact *false*. Most of the outer cluster is moving in tangential orbits that should not be affected by a redistribution of the interior mass. However, even in the outer layers, there are some orbits that penetrate to small distances, allowing the stars to be captured. This increase in the interior mass leads to changes in the outer orbits, so that the process can continue. The possibility of this "avalanche-type contraction" was foreseen by Zel'dovich and Podurets (1965), and in § II we present evidence that it does in fact occur.

Several exact results are known concerning the stability of spherical Newtonian clusters. Curiously, most of these assume that the distribution function is a strictly decreasing function of the energy. We perform numerical experiments with Newtonian polytropic clusters in § II to explore cases in which the distribution function increases with energy.

If a bound cluster is initially not in equilibrium because its velocity dispersion ("temperature") is too low, it will contract, undergo "violent relaxation," and thermalize its velocity distribution (Lynden-Bell 1967). This collective thermalization mechanism is believed to be responsible for achieving relaxation in such collisionless systems as clusters of galaxies and elliptical galaxies. We discuss for the first time the phenomenon of violent relaxation in general relativity (§ III). We discuss the transition between violent relaxation, leading to virial equilibrium, and continued catastrophic collapse to a black hole. One interesting difference between general relativity and the Newtonian theory is that a homogeneous spherical configuration oscillates homologously forever in Newtonian theory. In general relativity, such a system can virialize via violent relaxation.

A number of astrophysical issues arise directly from these dynamical studies. For example, as mentioned above, a large fraction of the total cluster mass can end up in a black hole when an unstable centrally condensed cluster collapses. The collapse of dense star clusters thus provides a possible origin for quasars and active galactic nuclei (AGNs) (Shapiro and Tuekolsky 1985*b*, hereafter Paper III).

The possibility of relativistic violent relaxation is important if there exist collisionless particles with nonzero rest mass produced in the early universe. Clumps of such particles can collapse to black holes if their initial velocity dispersion is sufficiently small (see § III). These black holes are potential sites for hiding dark matter and missing mass.

II. EVOLUTION OF ISOTROPIC, EQUIVALENT CLUSTERS: SOME NUMERICAL EXAMPLES

In this section we summarize the dynamical behavior of initially isotropic, equilibrium configurations whose evolution we follow on the computer. The models described here are all constructed from isotropic, single-mass distribution functions of the form

$$\frac{dN}{d^3\hat{p}d^3\hat{x}d\mu} \equiv F(E, L, \mu) = f(E)\delta(\mu - \mu_0) . \tag{1}$$

In equation (1), $F(E, L, \mu)$ is the general spherical solution to the Vlasov equation in a static spherical spacetime; E is the conserved "energy at infinity" of a particle,

$$E \equiv -\boldsymbol{p} \cdot (\partial/\partial t) = -p_0 , \tag{2}$$

L is the conserved total angular momentum of a particle,

$$L \equiv r_s p^{\hat{T}} \equiv r_s[(p^{\hat{\theta}})^2 + (p^{\hat{\phi}})^2]^{1/2} , \tag{3}$$

and $\mu_0 = [(p^{\hat{0}})^2 - (p^{\hat{r}})^2 - (p^{\hat{\theta}})^2 - (p^{\hat{\phi}})^2]^{1/2}$ is the conserved rest mass of a particle (cf. Misner, Thorne, and Wheeler 1973, hereafter MTW, § 25.7, for a general discussion). Here carets denote phase space coordinates as measured in an orthonormal frame. Accordingly, $f(E)$ is the usual phase space density for an isotropic ensemble and $d^3\hat{x}d^3\hat{p}$ is the locally measured phase space volume element.

The cases chosen for numerical study were selected partly for historical reasons, i.e., to make contact with previous (mostly "analytic") work. However, they were also chosen because of their suitability for resolving points of principle or issues of particular physical relevance vis-à-vis the stability and ultimate fate of collisionless, equilibrium configurations in general relativity. Key features of the models we examine are summarized in Table 1 of Paper I (test-bed calculations, cases 10–14) and in Tables 1–4 below.

a) Truncated Maxwell-Boltzmann Distributions

i) *The Equilibrium Sequence*

We first consider the dynamical fate of a collisionless ensemble initially in equilibrium and characterized by a truncated Maxwell-Boltzmann, isothermal distribution function,

$$f(E) = \begin{cases} K \exp(-E/T) , & E \le E_{\max} , \\ 0, & E > E_{\max} . \end{cases} \tag{4}$$

Here K is a normalization constant, T is a constant "temperature," and $E_{\max}$ is the maximum allowed energy, corresponding to a particle momentarily at rest at the surface of the configuration, $r_s = R$. The energy cutoff $E_{\max}$ ensures that all particles are restricted to a finite region of space.

Physically, collisionless systems with truncated Boltzmann distributions are natural objects to study. In any real cluster, "thermalization" processes are always at work driving the system to an (unattainable) isothermal equilibrium. Thus, the central regions of elliptical galaxies and large clusters of galaxies like Coma have isothermal profiles, because of collisionless thermalization via "violent relaxation" (Lynden-Bell 1967). The cores of globular clusters have isothermal profiles, owing to collisional thermalization via the cumulative perturbative effect of distant, two-body, small-angle gravitational encounters (see, e.g., Spitzer 1975, 1985; Lightman and Shapiro 1978; Goodman and Hut 1985, for extensive reviews and references).

Relativistic star clusters in equilibrium with truncated Boltzmann distributions have been extensively studied in the literature. Models of truncated isothermal clusters have been constructed by Zel'dovich and Podurets (1965); Fackerell (1966), Ipser (1969), and Katz, Horwitz, and Klapisch (1975). The dynamic stability of these clusters to radial perturbations was first examined by Ipser (1969), who employed a trial function in a variational principle to determine the normal modes of radial pulsations. The stability was later reexamined by Suffern and Fackerell (1976), who refined the trial functions of Ipser (1969). The result of these studies was the finding that all truncated isothermal clusters with central redshifts $z_c \gtrsim 0.5$ are dynamically unstable. To within the numerical accuracy of the stability calculations, the point of maximum binding energy along suitable equilibrium sequences of truncated isothermal configurations *coincides* with the point past which all models are known to be unstable. Ipser (1980) thus argued that this result provided evidence that the sufficient condition for stability which he was able to prove, namely, that configurations below the first binding-energy maximum are stable, is also necessary. Specifically, he speculated that "instability to collisionless spherical perturbations sets in at precisely the first binding-energy maximum along appropriately constructed sequences."

We have reconstructed the equilibrium sequences of truncated isothermal spheres considered by Zel'dovich and Podurets (1965) and Ipser (1969) and have employed the results as initial data in our dynamical code. Our numerical integrations of the collisionless, isotropic equilibrium equations closely follow the procedure of Fackerell (1966) and Ipser (1969). All nondimensional features of a cluster are specified by only two nontrivial parameters, e.g., $\tilde{T} \equiv T/\mu_0$ and $\tilde{E}_{\max} = E_{\max}/\mu_0$ (see MTW, Box 25.9). For computational purposes it is more convenient to specify two different parameters, arrived at as follows. Suppose we write the line element in standard Schwarzschild coordinates,

$$ds^2 = -e^{2\Phi}dt^2 + e^{2\Lambda}dr_s^2 + r_s^2(d\theta^2 + \sin^2\theta d\phi^2) . \quad (5)$$

Next we specify a value for $y_c \equiv e^{2\Phi(0)}/\beta$, the central-to-surface redshift factor (i.e., $y_c^{-1/2} - 1$ is the redshift of a photon emitted at the cluster's center and received at the surface). Here we define $\beta \equiv e^{2\Phi(R)} = 1 - 2M/R$, where M is the total mass energy of the configuration, and R is the coordinate radius of the surface. Finally, we specify a value for the quantity $T' \equiv T/(\mu_0 \beta^{1/2})$, the temperature as measured by an observer at the surface of the configuration divided by the particle's rest mass.

When written in an appropriate nondimensional form, the equilibrium field equations (see Ipser 1969, eqns. [33]–[37]) do not contain β. However, once the field equations have been solved for a given y_c and T', quantities like

$$z_c = (\beta y_c)^{-1/2} - 1 , \quad \tilde{T} = T'\beta^{1/2} , \quad \tilde{E}_{\max} = \beta^{1/2}$$

and the fractional binding energy

$$E_b/M_0 \equiv (M_0 - M)/M_0 \quad (6)$$

are uniquely determined (here M_0 is the *rest* mass-energy of the configuration). Note that β is unknown before the structure of the cluster has been determined.

Following Zel'dovich and Podurets (1965) and Ipser (1969), we shall consider the *one-parameter* equilibrium sequence defined by

$$\tilde{E}_{\max} = 1 - (1/2)\tilde{T} . \quad (7)$$

This constraint induces a unique relationship between the two parameters y_c and T'. They thus can no longer be chosen independently. Values for each pair (y_c, T') along the sequence specified by equation (7) were found numerically by Ipser (1969, see his Table 1). We employed these same pairs of values in recomputing our equilibrium cluster models; our results, which agree closely with those of Ipser (1969), are summarized in columns (3)–(6) of Table 1. For a more detailed description of these equilibrium models, including expressions for the equilibrium pressure, total mass-energy density, and rest mass density, the reader is referred to Ipser's (1969) paper. For a discussion of how the cluster models are implemented as initial data in our dynamical code, see Paper I, § V. Note that in the Newtonian limit, $y_c - 1 \ll 1$ and $T' \ll 1$.

ii) *The Numerical Transition from Stability to Instability*

We have evolved all the clusters in Table 1 on the computer to determine their nonlinear dynamical behavior with time. Their final fates are summarized in the last column in Table 1 as well as in Figure 1. In the figure we plot for this sequence the fractional binding energy E_b/M_0 and ω^2/ρ_c, the square of the frequency of oscillation of the fundamental radial mode divided by the central mass-energy density, versus central redshift z_c. The values of ω^2/ρ_c appearing in Table 1 and Figure 1 were taken from Ipser (1969), who obtained them numerically from a variational principle. Figure 1 is essentially the same as Figure 2 of Ipser (1969) (see also the figure in MTW, Box 25.9) with one very notable addition: the points identifying particular models along the equilibrium sequence are now coded to reveal their ultimate dynamical fate when followed by our fully nonlinear computer calculations.

In general, we can identify four generic types of late-time evolutionary behavior, as illustrated by the four spacetime diagrams plotted in Figure 2. Configurations with low $z_c \lesssim 0.4$ are all dynamically stable. Model *a* in Figure 2, corresponding to the equilibrium model with (y_c, T') = (0.840, 0.105) in Table 1 and Figure 1, is the prototype for these stable clusters. With a modest choice of integration accuracy parameters (the same set employed for the homogeneous circular orbit clusters described in Paper I, § VII*b*), this cluster conserved its global relativistic energy E_0 to within 4%, after evolving for over 50 central free-fall time scales. This diagnostic energy parameter is defined in equation (50) of Paper I and is rigorously conserved in truly static space times.

Configurations with high z_c, $\gtrsim 0.4$, on the other hand, are found to be dynamically unstable. Model *b*, with (y_c, T') = (0.556, 0.262), collapses to form a black hole in a few dynamical time scales. For comparison, note that the initial *central* free-fall time scale for this configuration is $t_{\rm ff}/M = 8.6$, while the

TABLE 1

MAXWELL-BOLTZMANN (isothermal) EQUILIBRIUM SEQUENCE[a]

y_c[b] (1)	T'[b] (2)	z_c (3)	E_b/M_0 (4)	R/M (5)	$\langle\rho\rangle/\rho_c$ (6)	ω^2/ρ_c[c] (7)	Dynamical Fate (8)
0.923......	0.0512	0.068	+0.0108	40.5	0.123	+1.17	Stable equilibrium
0.840......	0.105	0.148	+0.0205	20.6	0.113	+0.879	Stable equilibrium
0.638......	0.222	0.391	+0.0347	10.5	0.085	+0.181	Stable equilibrium
0.616......	0.235	0.423	+0.0353	10.1	0.0816	+0.123	Collapse to black hole
0.592......	0.247	0.459	+0.0356	9.66	0.0779	+0.065	Collapse to black hole
0.556......	0.262	0.517	+0.0357	9.16	0.0718	−0.016	Collapse to black hole
0.531......	0.272	0.559	+0.0353	8.87	0.0676	−0.068	Collapse to black hole
0.487......	0.288	0.640	+0.0338	8.46	0.0599	−0.144	Collapse to black hole
0.395......	0.312	0.839	+0.0265	7.95	0.0432	< −0.257	Collapse to black hole
0.309......	0.312	1.08	+0.0132	7.94	0.0269	< −0.295	Expansion, reimplosion, and oscillation
0.239......	0.286	1.34	−0.0027	8.52	0.0141	< −0.303	Collapse to black hole
0.179......	0.223	1.63	−0.0152	10.4	0.0045	< −0.243	Expansion to infinity

[a] $f(E) = K \exp(-E/T)$ for $E \le E_{\max}$, and $f = 0$ for $E > E_{\max}$, where K and T are constants.

[b] Pair of values (y_c, T) uniquely specifies a member of the sequence defined by eq. (7); from Ipser 1969.

[c] Trial-function eigenfrequency of lowest radial mode, in units of ρ_c; from Ipser 1969.

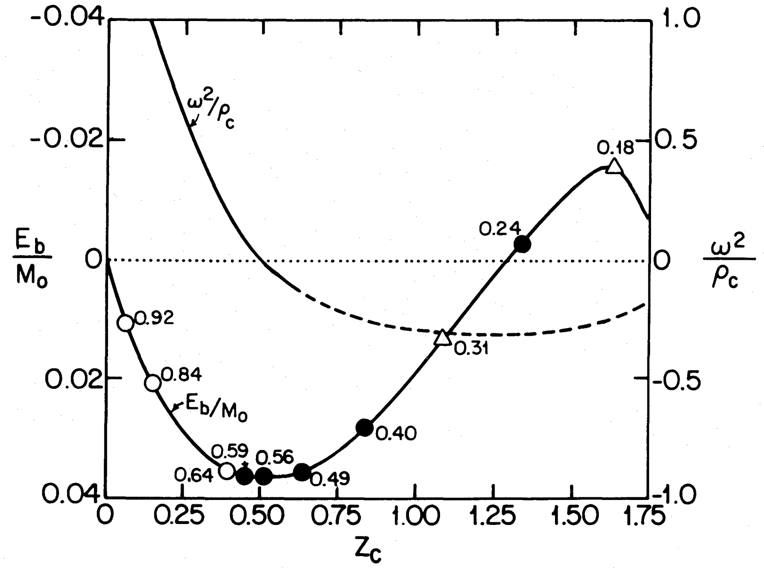

FIG. 1.—Maxwell-Boltzmann equilibrium sequence. The fractional binding energy E_b/M_0 and oscillation frequency ω^2 of the fundamental radial mode are plotted as functions of central redshift z_c. Clusters along the sequence are labeled by their values of y_c (see Table 1). Their dynamical fates are coded as follows: open circles indicate stable equilibrium; filled circles indicate collapse to a black hole; open triangles indicate unstable oscillations. (Equilibrium data after Ipser 1969).

initial *mean* free-fall time is $\bar{t}_{ff}/M = 32$. (Define $\bar{t}_{ff}/M$ by replacing ρ_{max} by $\langle\rho\rangle$ and setting $q \equiv 1$ in eq. [62] of Paper I). This collapse case is studied in detail below. Model *c*, specified by $(y_c, T') = (0.309, 0.312)$, undergoes large-amplitude, bound oscillations following an initial outward expansion. This unstable cluster ultimately relaxes to a new, less relativistic, equilibrium state, at which point it is no longer characterized by a truncated Maxwellian distribution function. Model *d*, with $(y_c, T') = (0.179, 0.223)$, also expands unstably outward initially. However, this model is *unbound*, since $E_b < 0$ (see Fig. 1). Hence, it is not surprising that this configuration continues to expand outward without recollapsing; it will ultimately disperse to infinity with nonzero kinetic energy.

The different dynamical behavior patterns revealed along the truncated isothermal sequence closely mimic the different trends found along the equilibrium sequence of clusters with homogeneous profiles and circular orbits already discussed in Paper I. (See § VII*b* and especially Fig. 10 therein; this circular orbit sequence is parameterized by the ratio R/M, the cluster radius divided by the total mass-energy). The possibility of finite collisionless equilibrium configurations with *negative* binding energy is a purely relativistic phenomenon: in Newtonian theory, the virial theroem requires $E_b = -W/2 > 0$, where W is the gravitational potential energy. The possibility of equilibrium configurations with negative binding energy was discussed by Zel'dovich and Novikov (1971) in the context of relativistic, spherical *fluid* stars. They argued that such configurations must reside deep inside the unstable domain of an equilibrium sequence, since the transition from stability to instability occurs at the point of maximum (positive) binding energy. Unstable configurations just beyond the transition point are bound; consequently, they ultimately must undergo catastrophic collapse, even if at $t = 0$ they are subject to small perturbations which cause them to slightly expand initially. By contrast, unstable configurations with negative binding energy can either collapse *or* expand indefinitely, depending on the initial spectrum of small perturbations. When the mass of the star is dispersed in the case of continuous expansion, the matter arrives at infinity with positive kinetic energy.

Our computer calculations show that unstable *collisionless* equilibrium spheres exhibit analogous dynamical behavior to unstable fluid stars. Specifically, all clusters beyond the point of maximum binding energy appear to be unstable. Unstable configurations just beyond the critical point ($z_c \approx 0.42$ in Fig. 1) invariably collapse to black holes. Unstable configurations deep inside the unstable domain undergo either catastrophic collapse or expansion, depending on the initial perturbations ($\equiv$ numerical roundoff in the initial data in our computer simulations). If bound (i.e., $E_b > 0$), configurations that initially expand must ultimately reimplode. However, they can settle into new equilibrium states in a few dynamical times following "violent relaxation" if the postcollapse oscillations are sufficiently large-amplitude and nonhomologous (see § III). (Unstable, bound *fluid* stars can exhibit behavior similar to "violent relaxation": large-amplitude, nonhomologous oscillations following adiabatic collapse can lead to shock heating, which enables initially cold stars to establish new, "hot" equilibrium states and avoid catastrophic collapse, no matter what their mass. See Shapiro and Teukolsky 1980 for numerical demonstrations.) If unbound (i.e., $E_b < 0$), however, the initially expanding configurations need not reimplode and can expand forever to infinity. Unstable models *b*–*d* illustrate all three of these possibilities.

A key question remains to be discussed: *to what extent does our numerical location of the transition point to dynamical instability along the truncated isothermal equilibrium sequence conform to prior theoretical expectations?* First, we note with satisfaction that *all* models with fundamental eigenfrequencies satisfying $\omega^2/\rho_c < 0$ are found to be unstable. In addition, two models near the transition point with ω^2/ρ_c small, but nevertheless positive, also collapse unstably to black holes (see Table 1). Some experimentation with our integration input accuracy parameters (see Paper I) in this region convinces us that this numerical finding may in fact be real. Nevertheless, these

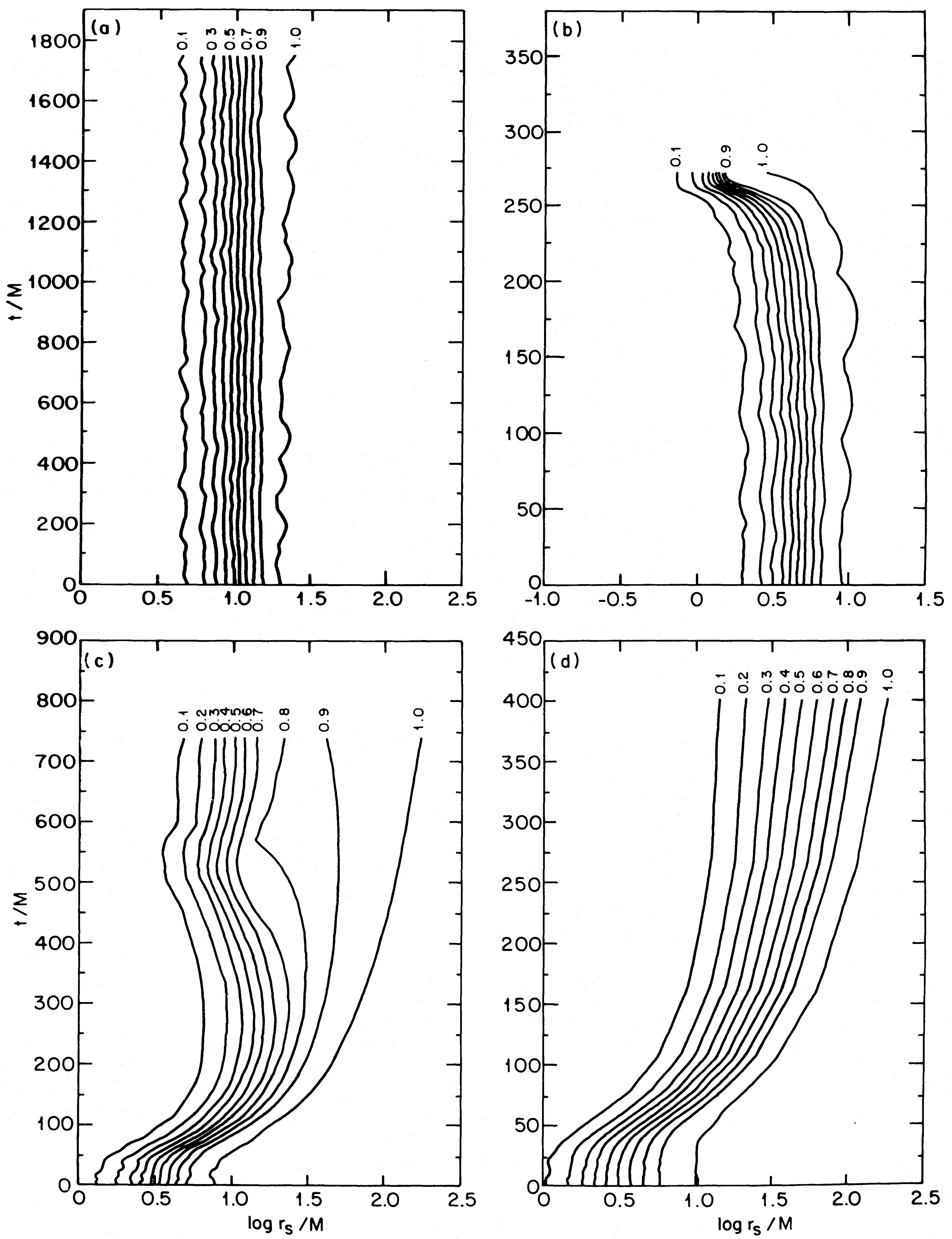

FIG. 2.—Spacetime diagrams for Maxwell-Boltzmann clusters initially in equilibrium. The solid lines are the world lines of fictitious Lagrangian matter tracers labeled by their fixed interior rest-mass fraction. Model *a*, with $(y_c, T') = (0.840, 0.105)$, is in stable equilibrium. Model *b*, with $(y_c, T') = (0.556, 0.262)$, collapses to a black hole. Model *c*, with $(y_c, T') = (0.309, 0.312)$, undergoes unstable, bounded oscillations. Model *d*, with $(y_c, T') = (0.179, 0.223)$, expands unstably to infinity.

results are fully consistent with theoretical expectations, since the trial function employed by Ipser (1969) to determine ω^2 only provides a sufficient, and not a necessary, condition for instability. Hence other trial functions, closer to optimal, should identify modes where ω^2 is negative for these two unstable configurations. We note, however, that the two models in question also reside just outside the region of dynamic instability, as rediagnosed by Suffern and Fackerell (1976, see their Fig. 1). But again, these authors adopted the trial function method of Fackerell (1970), which only provides a *sufficient* criterion for dynamical instability.

What about the role of the maximal fractional binding energy as the location of the transition point from stability to instability? A glance at Table 1 and Figure 1 reveals that the transition point as determined by our numerical integrations certainly lies *close to* the first maximum of the binding energy along the sequence defined by equation (7). Unfortunately, as Ipser (1980) has emphasized, his powerful *sufficient* condition that members of *appropriate* equilibrium sequences are stable at least up to the first maximum of the binding energy does not quite apply to this particular sequence for technical reasons implicit in his proof. Perhaps due to this, the two unstable models mentioned above reside *just below* the maximal point on the binding energy curve on the descending "stable" branch. (Alternatively, slight numerical inaccuracy may easily account for this result). In any case, rigorous verification of Ipser's (1980) sufficient condition and his speculation that it is also necessary must be postponed to the subsequent sections, where we shall consider "suitable" equilibrium sequences for which his theorem applies.

iii) *Collisionless Collapse to a Black Hole*

The most interesting general relativistic phenomenon involving collisionless clusters is the catastrophic collapse to a black hole of a marginally unstable, equilibrium configuration. Model *b* in Figure 2 (the sixth entry in Table 1) provides a good illustration.

The geometry of the collapse is probed in Figure 3, which is a blowup of the spacetime diagram of Figure 2*b* at late times. The dotted lines are the world lines of the imaginary Lagrangian tracers in the cluster, labeled by their interior rest-mass fraction (note: *no* particles in the cluster actually follow such trajectories). The solid lines show the trajectories of outgoing radial light rays emitted from various radii at various times. By finding pairs of light rays emitted from the same radius, one of which escapes and one of which does not, we can trace the growth of the event horizon (*dashed line*) as more and more of the matter flows into the black hole.

The shaded portion of the diagram represents the region of trapped surfaces, where even an outgoing spherical flash of light immediately becomes a sphere of smaller area. The apparent horizon (outermost trapped surface) always lies inside the horizon, in accordance with theorems on black hole horizons (Hawking and Ellis 1973).

Virtually all the rest mass (99.9%) lies inside the event horizon by the end of the calculation at $t/M = 272$. The residual mass lies just outside the horizon and is moving inward. The apparent and event horizons essentially coincide by this time, both lying quite close to $r_s = 2M$, as they must. (The apparent horizon is within 1% of $r_s = 2M$ at $t/M = 272$.) By this time the central lapse has fallen to $\alpha_c = 4.8 \times 10^{-4}$, as shown in Figure 4. This exponential "collapse of the lapse" (Smarr and York 1978) at late times is the result of maximal

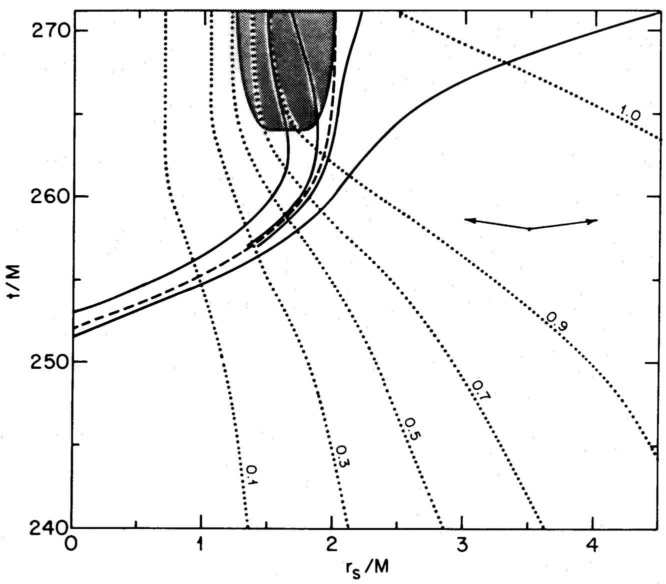

FIG. 3.—Spacetime diagram for the Maxwell-Boltzmann cluster shown in Fig. 2*b*. The dotted lines are the world lines of fictitious Lagrangian matter tracers labeled by the fixed interior rest-mass fraction. The dashed line is the event horizon. The solid lines are pairs of light rays emitted from the same radius at different times and used to locate the event horizon. The arrows show the propagation directions of inward and outward light rays at large distances from the black hole. The shaded area is the region of trapped surfaces.

slicing attempting to hold back proper time at the center to avoid the singularity. Accompanying the drop in α_c is a steep rise in the central conformal factor, which increases to $A_c = 290$ at the end of the integration. (Recall that in strict *Newtonian* gravity, values of α_c and A_c are $\alpha_c = 1 + \phi_c$, where ϕ_c is the central potential, and $A_c = 1$).

The almost vertical slope of the Lagrangian world lines inside the horizon is due to the appearance of a "limit surface," i.e., a two-dimensional spatial hypersurface which the outermost particles approach asymptotically at late times. (See Eardley and Smarr 1979; Petrich, Shapiro, and Teukolsky 1985; and Paper I, § VII*d* for a discussion of the limit surface arising in Friedmann dust collapse.) The appearance of a limit surface is a characteristic feature of spherical collapse to a black hole in the maximal slicing gauge.

Our integrations proceed smoothly without the appearance of physical or numerical singularities. We terminate them at late times whenever the central dynamical time scale becomes sufficiently small that it becomes prohibitively time-consuming to continue following the particle orbits near $r = 0$ with any reliability. Typically, for clusters like model *b*, which are initially not very centrally condensed (i.e., $\langle\rho\rangle/\rho_c \gtrsim 10^{-3}$), the evolution is essentially completed by this time, as virtually all the matter is inside $r_s = 2M$.

Matter profiles for this case are plotted in Figures 5–7 on various time slices during the collapse. The rest-mass density profile as measured by normal observers (defined in text above eq. [68] of Paper I) is shown in Figure 5. The density profile grows somewhat more centrally condensed during the collapse. As the cluster radius collapses from $r_s = R = 9M$ to $r_s \lesssim 2M$, the profile preserves its truncated isothermal shape. The velocity dispersion, or "temperature" as measured by locally comoving observers (eq. [59] of Paper I) is plotted in Figure 6. Initially, the total velocity dispersion varies from a peak of $\langle v\rangle = 0.5$ at the center, to $\langle v\rangle = 0.3$ at the radius containing

1985ApJ...298...58S

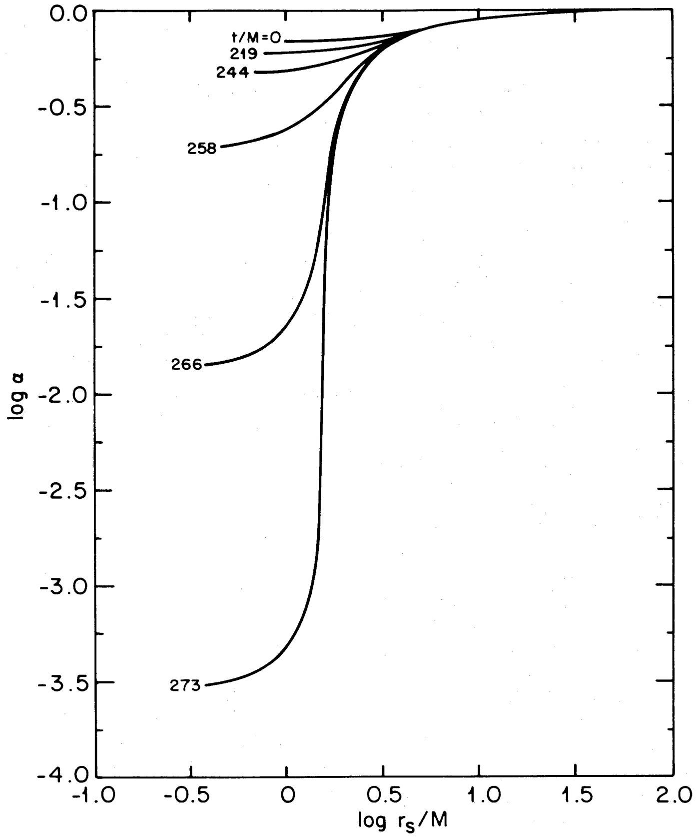

FIG. 4.—The lapse function α as a function of areal radius r_s on selected time slices for the Maxwell-Boltzmann cluster shown in Fig. 2*b*

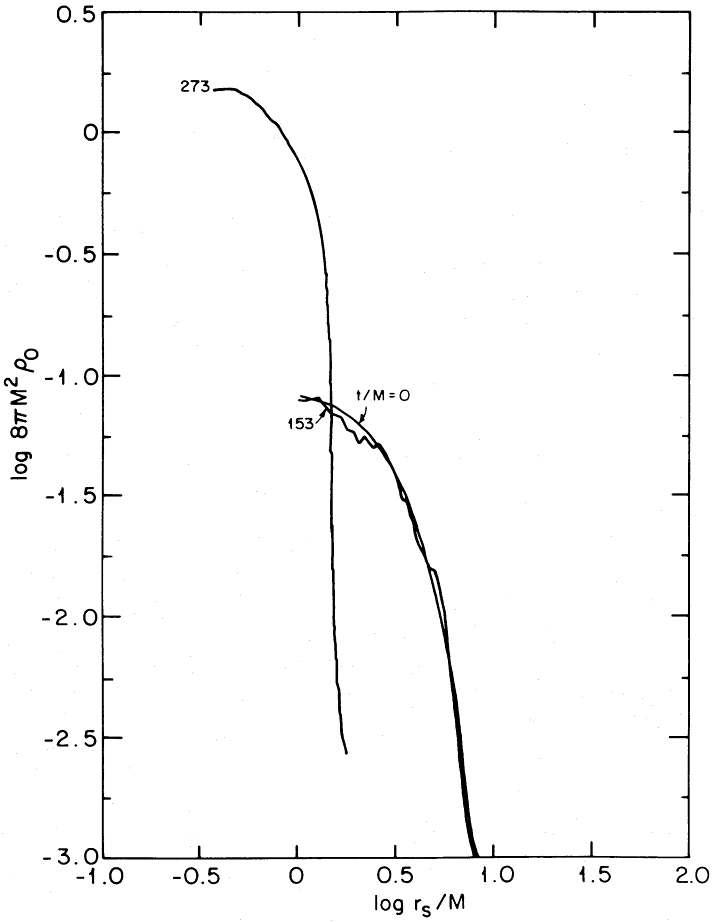

FIG. 5.—The rest-mass density ρ_0 as measured by a normal observer for the case described in Fig. 4

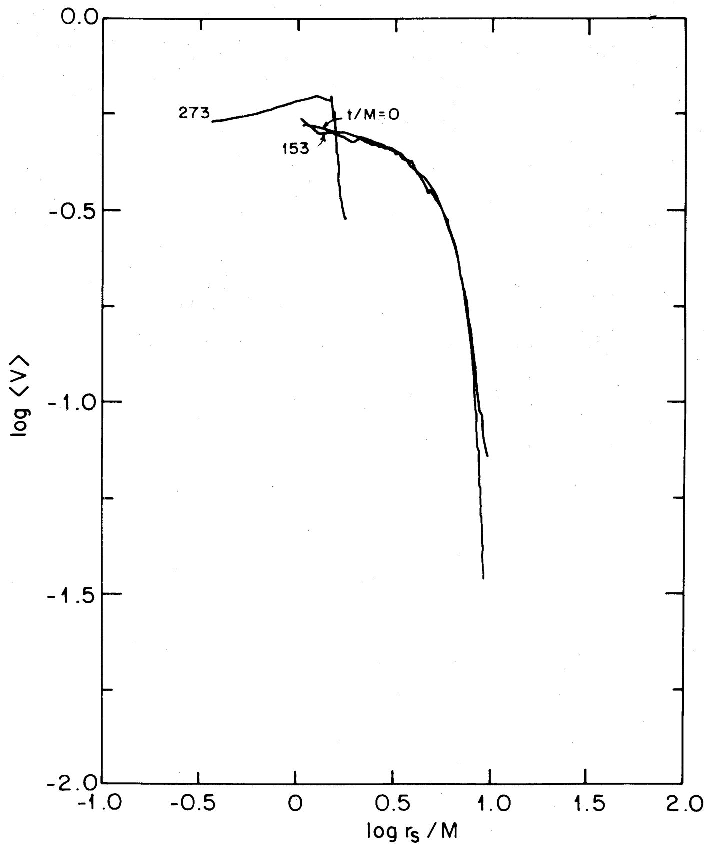

FIG. 6.—The velocity dispersion $\langle v \rangle$ for the case described in Fig. 4

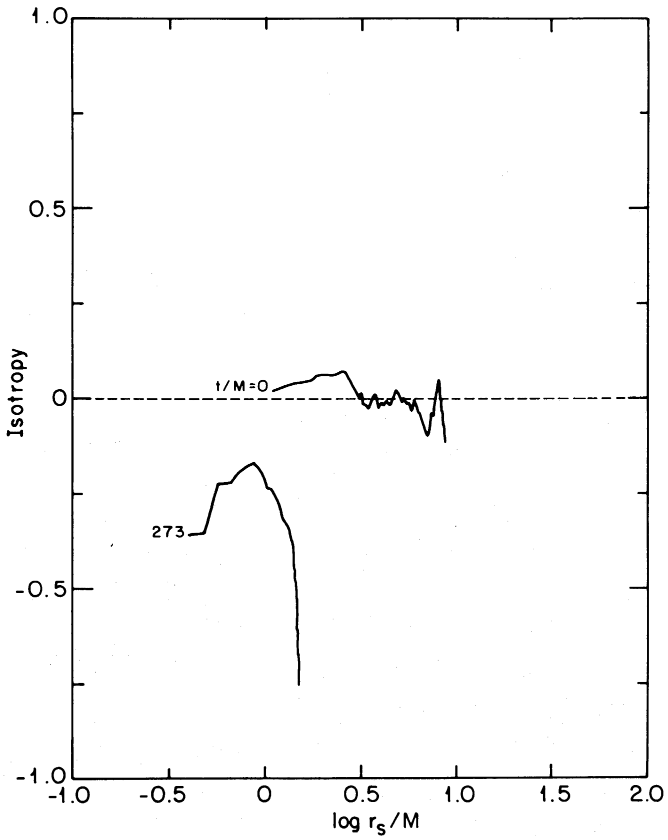

FIG. 7.—The isotropy measure for the case described in Fig. 4

90% of the rest mass, to $\langle v \rangle = 0$ at the surface. At $t/M = 273$, the velocity is even more uniform across the matter, varying from $\langle v \rangle = 0.7$ at the center to $\langle v \rangle = 0.6$ at the 90% radius. Initially isotropic, the comoving velocity profile grows anisotropic with time, as is evident from Figure 7. The comoving isotropy parameter (eq. [61] of Paper I) is constructed to be 0 for isotropic (or dust) velocity profiles, $+1$ for purely radial profiles, and -1 for purely tangential profiles. At late times, the particle motions beocome increasingly tangential. The freezing of particles in the radial direction is related to the appearance of a limit surface and is due to the success of maximal slicing in holding back the collapse. Of course, all the matter profiles described above are both gauge- and frame-dependent, so their physical significance should not be overemphasized.

Snapshots of the cluster are shown at various times during the collapse in Figure 8. At late times the configuration is clearly seen to collapse inside its event horizon at $2M$. The surface approaches a limit surface at approximately $1.5M$. A blowup of the central regions for the same time is shown in Figure 9.

b) *Monoenergetic Distributions*

i) *The Equilibrium Sequence*

Because of their mathematical simplicity, we have considered the dynamical evolution of equilibrium models constructed from a monoenergetic phase space distribution function. The distribution is given by equation (1) with

$$f(E) = K\delta(E - E_{\max}) , \tag{8}$$

where K is a normalization constant and $E_{\max}$ is the constant

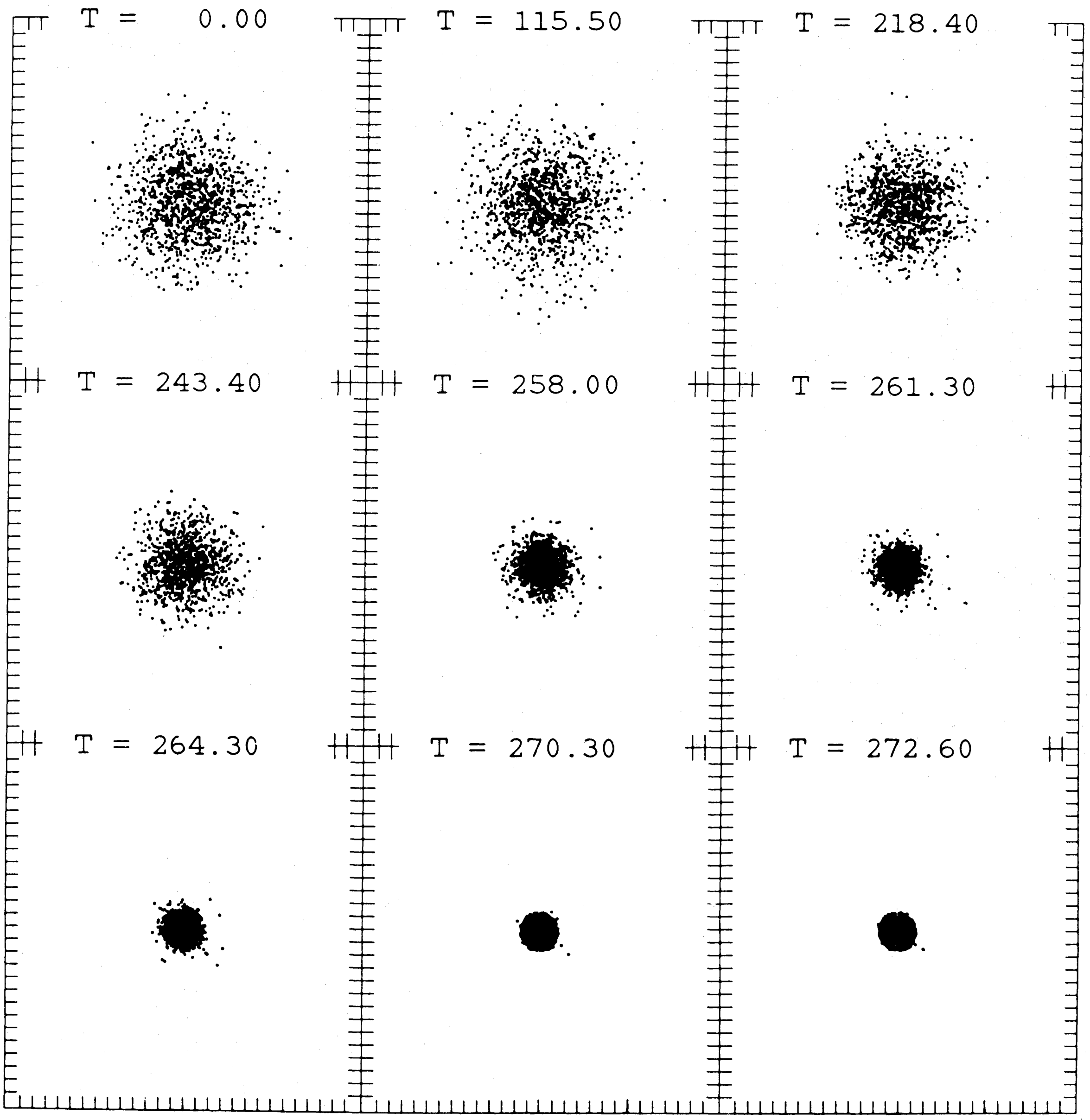

FIG. 8.—Snapshots of the cluster for the case described in Fig. 4. Each frame is labeled by the time in units of M. The spatial grid markers correspond to 1 M in areal radius.

"energy at infinity" of every particle in the configuration. To construct the equilibrium models we again followed the numerical procedure of Fackerell (1966) and Ipser (1969) outlined in § II*a* for the truncated isothermal sequence. Two simplifications, due to the uncomplicated nature of equation (8), facilitate the process. First, the moment equations for ρ, ρ_0, and P, given $f(E)$, can be integrated analytically. This greatly accelerates the integration of the collisionless equilibrium equations. Second, the nondimensional structure of a cluster can be uniquely specified by a *single* nontrivial parameter, like y_c. Consequently, a monoenergetic equilibrium sequence is parameterized by y_c with no additional imposed constraints.

Following Zel'dovich and Novikov (1971), we remark that in the *Newtonian* limit, $y_c - 1 \ll 1$, a monoenergetic distribution corresponds to a polytrope of index $n = 0.5$. In this case the matter pressure varies with density according to $P \propto \rho_0{}^{\Gamma}$, $\Gamma = 1 + 1/n = 3$. Collisionless polytropes with $\Gamma > 3$ or $n < 0.5$ do not exist, due to the condition that the distribution function must everywhere satisfy $f(E) \geq 0$.

ii) *The Numerical Transition from Stability to Instability*

We have constructed the monoenergetic equilibrium sequence described above and employed it as initial data in our simulation code. The fractional binding energy versus central redshift along the sequence is plotted in Figure 10. Also indicated on this plot are the fates of four models which were evolved on the computer. The properties of these models are summarized in Table 2. Because the spacetime diagrams and associated matter and metric profiles for these cases are qualitatively similar to those shown in § II*a* for the corresponding truncated isothermal models, we omit them here.

Figure 10 provides strong numerical evidence that insta-

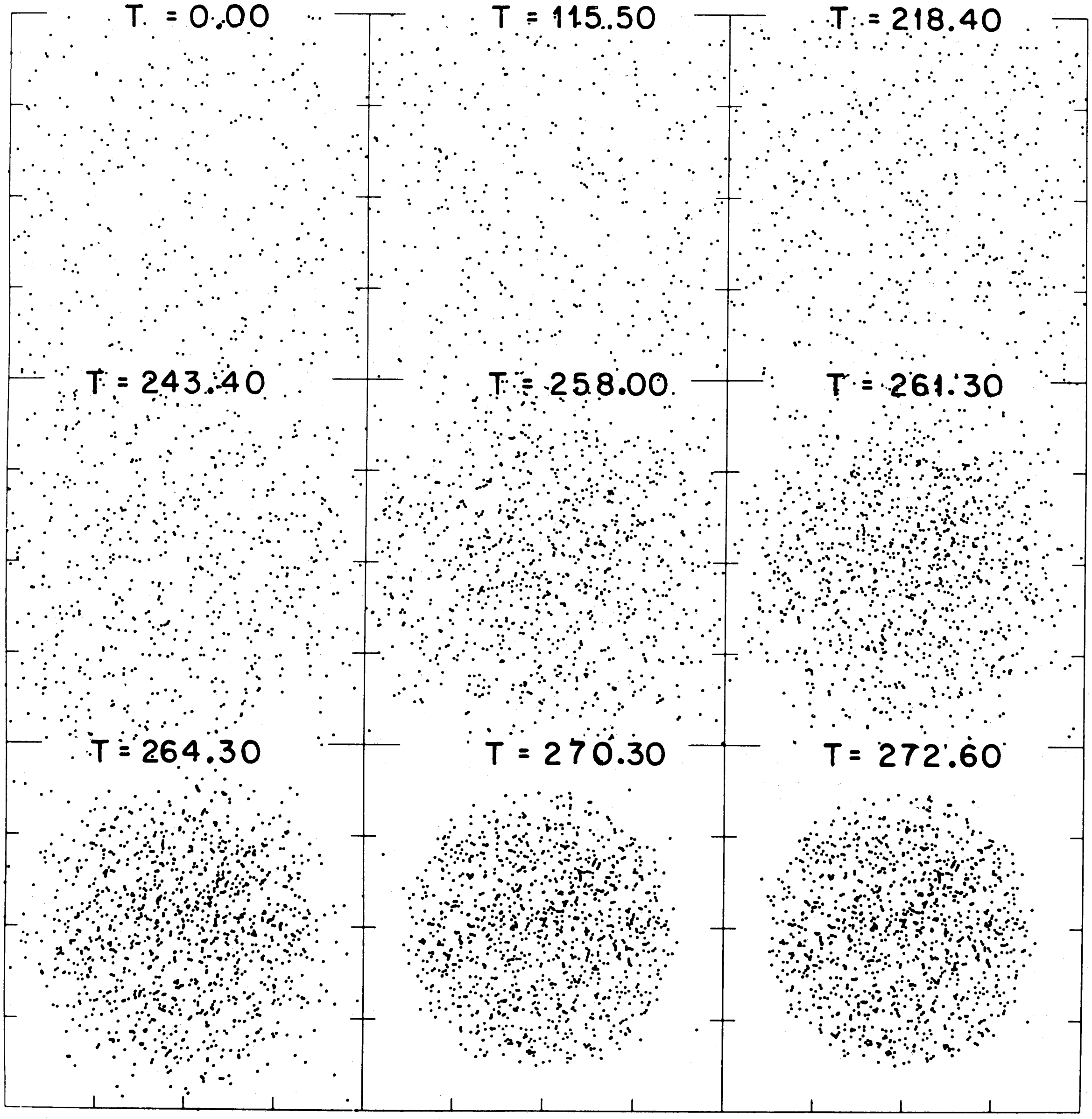

FIG. 9.—Blowup of the central regions shown in Fig. 8. Note that virtually all the mass lies inside the event horizon at $r_s/M = 2$ at late times. The surface approaches an asymptotic limit near $r_s/M \approx 1.5$.

TABLE 2

MONOENERGETIC EQUILIBRIUM SEQUENCE[a]

y_c[b]	z_c	E_b/M_0	R/M	$\langle\rho\rangle/\rho_c$	Dynamical Fate
0.900......	0.125	+0.0191	16.4	0.488	Stable equilibrium
0.819......	0.236	+0.0293	9.95	0.441	Stable equilibrium
0.605......	0.592	+0.0340	5.75	0.314	Collapse to black hole
0.283......	1.500	−0.0397	4.58	0.113	Collapse to black hole

[a] $f(E) = K\delta(E - E_{max})$, where K is a constant.

[b] Relativity parameter y_c uniquely specifies a member of the sequence.

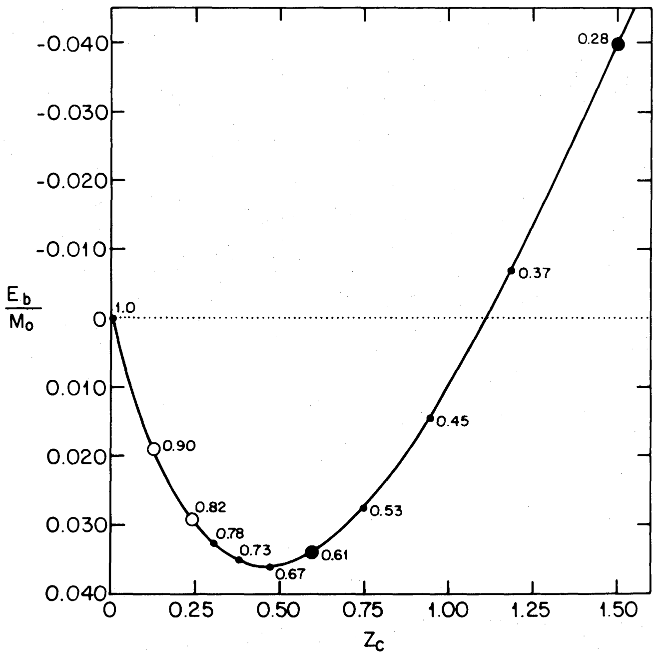

FIG. 10.—Monoenergetic equilibrium sequence. The fractional binding energy E_b/M_0 is plotted as a function of central redshift z_c. Clusters along the sequence are labeled by their value of y_c (see Table 2). The dynamical fates of four models along the sequence are coded as in Fig. 1.

bility to collisionless spherical perturbations sets in at precisely the first maximum in the binding energy curve for this sequence. Further numerical justification for this conclusion is provided by the additional examples discussed immediately below.

c) *Power-Law Distributions*

i) *Motivation*

It is of considerable computational and astrophysical interest to consider the dynamical fate of equilibrium models constructed from power-law distribution functions of the form

$$f(E) = \begin{cases} K[(E/E_{\max})^2]^{-\delta}[1 - (E/E_{\max})^2]^{\delta}\,, & E \le E_{\max} \\ 0, & E > E_{\max}\,, \end{cases} \tag{9}$$

where K, $E_{\max}$, and δ are constants. Interest in such configurations stems from a number of issues. First, the particular case $\delta \equiv 5/2$ was shown by Fackerell (1970) to be the exact solution for a polytropic, relativistic star cluster of index $n = 4$ and $\Gamma = 5/4$. These clusters are important because, unlike the truncated isothermal models, they are characterized by extreme core-halo density distributions (i.e., strong central concentration) near the first binding-energy maximum. For this reason, Fackerell (1970) has explored these configurations in considerable detail. He transformed the original variational principle of Ipser (1969) to a form that optimizes the trial functions used by Ipser to permit an analysis of the stability of such centrally condensed configurations. By estimating the lowest mode of radial pulsations from these trial functions, he obtained a simple sufficient criterion for their instability. Specifically, he showed that an $n = 4$ polytropic cluster is unstable if the central redshift satisfies $z_c > 0.730$. Such a cluster has a mean density divided by central density equal to 1.6×10^{-13}. The result is intriguing, because the first fractional binding-energy maximum occurs much earlier along the $n = 4$ polytropic equilibrium sequence, at $z_c \approx 0.41$. Fackerell's method, though quite powerful, cannot predict whether the equilibrium configurations in the intervening region are stable. Below, we show how our simulation code answers this question (the answer is that they are *not* stable!).

Apart from their unique computational aspects, extreme core-halo configurations are of significant astrophysical relevance. As is detailed in Paper III, *if relativistic star clusters form in nature, they are likely to be very centrally condensed.* Beginning from a dense, but otherwise Newtonian, state, and following secular core contraction on a two-body relaxation time scale (i.e., the "gravothermal catastrophe"), the core of a sufficiently massive cluster of neutron stars or stellar-mass black holes can evolve to an unstable relativistic state in a Hubble time. Such a cluster invariably has appreciable central concentration by the time it reaches a relativistic state. Ultimately it will undergo catastrophic collapse on a dynamical time scale to a supermassive black hole. The nature of the collapse and the size of the resulting black hole in the case of such an extreme core-halo configuration is a crucial issue. The outcome, which we consider below, may provide the basis for a natural mechanism for the formation of supermassive black holes believed to power AGNs and quasars.

Another significant issue concerning power-law clusters of the form given by equation (9) involves their dynamical stability in the *Newtonian* limit. Quite apart from any relativistic instabilities, the strictly Newtonian behavior of all power-law equilibrium configurations has not been rigorously established. General theorems guaranteeing the stability of collisionless, Newtonian spherical configurations only apply to a limited range of the parameter δ appearing in equation (9) [specifically, those for which $f'(E) < 0$, i.e., $\delta > 0$][1]. Indeed, Zel'dovich and Novikov (1971) have speculated that *all* Newtonian, power-law equilibria in the allowed range $-1 < \delta < 0$ are probably unstable. Numerical calculations are clearly required to address this matter, and we do so below by applying our code in the Newtonian regime.

ii) *Relativistic Polytropes with* $n = 4, \Gamma = 5/4$

a) Numerical transition from stability to instability: the binding-energy criterion.—Setting $\delta = 5/4$ in equation (9), we have reconstructed the $n = 4$, relativistic, polytropic equilibrium sequence originally examined by Fackerell (1970). We again employed the method of Fackerell (1966) and Ipser (1969) to integrate the nondimensional equilibrium equations. In doing so we took full advantage of Fackerell's (1970) equations (50), (51), and (53), which provide analytic expressions for the pressure P, mass-energy density ρ, and rest-mass density ρ_0. (Note that the coefficient 5^{-4} in his eq. [51] should be 5^{-5}.) In nondimensional form, the models can again be specified by a single nontrivial parameter, e.g., y_c or, equivalently, Fackerell's parameter α, which is related to y_c via $y_c \equiv (1 + 5\alpha)^{-2}$. In the Newtonian limit, $\alpha \ll 1$.

Our results (which agree closely with those of Fackerell) are summarized in Figure 11 and Table 3 (see Fackerell 1970 for a more extensive table of equilibrium models). Plotted in the figure is E_b/M_0 versus z_c along the equilibrium sequence. Also shown are the values along the sequence of the squared frequency ω^2, in units of $\tau \equiv \rho_c - 4P_c$, of the lowest mode of radial pulsations of the cluster as determined by Fackerell

[1] Recently, Sobouti (1984) has reported a proof for the case $f'(E) > 0$. Polytropes with $-1 < \delta < 0$ are stable, according to this proof.

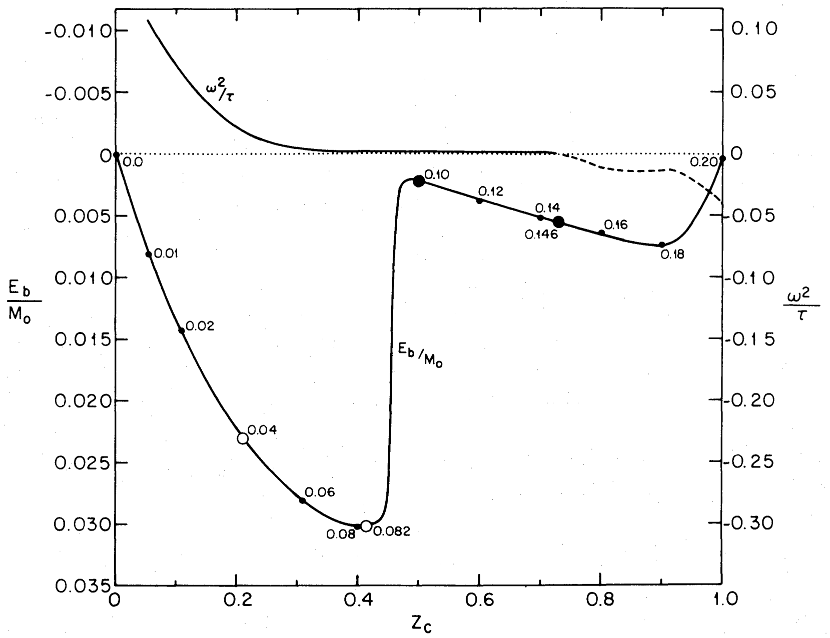

FIG. 11.—The $n = 4$ polytropic sequence. The fractional binding energy E_b/M_0 and oscillation frequency ω^2 in units of $\tau = \rho_c - 4P_c$ are plotted as functions of central redshift z_c. Clusters along the sequence are labeled by their value of α (see Table 3). The dynamical fates of four models along the sequence are coded as in Fig. 1. (Equilibrium data after Fackerell 1970).

using trial functions in perturbation equations. For $\alpha \geq 0.146$ the negative values calculated for ω^2/τ are merely upper bounds. Indicated on the binding energy curve, and highlighted in Table 3, are the dynamical fates of four clusters whose evolution we tracked with our computer simulation code.

Due to the extraordinary degree of central condensation characterizing these models (see Table 3), we employed a more stringent set of integration accuracy parameters than the standard set used in most of our previous calculations (see Paper I, § VII*b*). In particular, we used $N_f = 360$ radial grid points to cover the spatial mesh (of which 300 followed the matter distribution), and we followed $N_p = 5{,}980$ particles. The time step parameter q was fixed at 0.1. To check our results, we redetermined several spacetimes using $N_f = 660$ zones (of which 600 followed the matter) and $N_p = 11{,}980$ particles and obtained identical outcomes. In addition, all our external consistency checks (e.g., constancy of the exterior mass M as gleaned from eq. [47] of Paper I) were monitored carefully and behaved extremely well. Accordingly, in spite of the extreme core-halo density profiles characterizing these models, we believe that our numerical results are quite accurate and our conclusions reliable.

Our findings provide compelling numerical evidence that the conjecture of Ipser (1980), that *instability to collisionless spherical perturbations sets in precisely at the first fractional binding-energy maximum along appropriately constructed sequences*, is in fact true. Our conclusion is based on Figure 11, where the dynamical stability of an equilibrium model along such a sequence is seen to be remarkably sensitive to its location with respect to the first binding-energy maximum. This point corresponds to $z_c = 0.41$, while in fact Fackerell's (1970) trial functions do not yield negative values of ω^2 until $z_c = 0.73$, well beyond the fractional binding-energy maximum. Nevertheless, all configurations satisfying $z_c > 0.41$ are found to be unstable, including those in the intervening region $0.41 < z_c < 0.73$.

More than any other result this finding shows both the power and limitations of previous perturbative treatments of collisionless spherical configurations in general relativity. In all cases we have confirmed the sufficiency of their criterion for instability: all models with $\omega^2 < 0$ for some trial function are indeed unstable. Furthermore, all models up to the first maximum of the fractional binding energy are stable, which has been shown by Ipser (1980) to be a sufficient condition for stability for one-parameter sequences like relativistic polytropes. However, *perturbation theory does not yet provide a necessary criterion for instability* as well. The desired necessary and sufficient criterion must apparently focus on the first frac-

TABLE 3

POLYTROPIC EQUILIBRIUM SEQUENCE WITH $n = 4$, $\Gamma = 5/4$[a]

y_c[b]	α[b]	z_c	E_b/M_0	R/M	$\langle\rho\rangle/\rho_c$	ω^2/τ[c]	Dynamical Fate
0.694......	0.040	0.211	0.0231	1.16×10^2	1.48×10^{-4}	0.019	Stable equilibrium
0.503......	0.082	0.411	0.0302	1.73×10^3	7.19×10^{-9}	>0, <0.00015	Stable equilibrium
0.444......	0.100	0.500	0.00224	5.24×10^3	4.01×10^{-13}	>0, $<2.5 \times 10^{-9}$	Collapse to black hole
0.334......	0.146	0.730	0.00546	7.59×10^3	1.59×10^{-13}	$<-1.7 \times 10^{-3}$	Collapse to black hole

[a] $f(E) = K(E/E_{\max})^{-5}[1 - (E/E_{\max})^2]^{5/2}$ for $E \leq E_{\max}$ and $f = 0$ for $E > E_{\max}$, where K is a constant.
[b] Fackerell 1970 relativity parameter α related to y_c according to $y_c \equiv (1 + 5\alpha)^{-2}$; either parameter uniquely specifies a member of the sequence.
[c] Trial-function eigenfrequency of lowest radial mode, in units of $\tau \equiv \rho_c - 4P_c$; from Fackerell 1970.

tional binding-energy maximum, as in the case of equilibrium sequences of *fluid* stars. Proving such a theorem rigorously, though nontrivial, would be highly desirable. For now, our numerical results will have to suffice.

b) Collisionless collapse to a black hole: "Avalanche-type contraction."—Both the unstable models along the equilibrium sequence which we evolved on the computer collapsed to a black hole in a few dynamical time scales. Because of their extreme central concentrations, these configurations, and the black holes to which they give birth, are particularly significant.

Consider the unstable equilibrium configuration located just beyond the first fractional binding-energy maximum in Figure 11 with $z_c = 0.500$. It is an extreme core-halo configuration with $\langle\rho\rangle/\rho_c = 4.01 \times 10^{-13}$. Its core is highly relativistic, with central lapse $\alpha_c = 0.67$ and central rms velocity dispersion $\langle v\rangle = 0.45$. Its halo, however, is not relativistic; at the half rest-mass radius $r_s/M = 3.6 \times 10^2$, the lapse and velocity dispersion are essentially Newtonian, with $\alpha = 0.998$ and $\langle v\rangle = 3.5 \times 10^{-2}$. The outer radius of the cluster is at a distance $r_s/M = RM = 5.2 \times 10^3$, at which point the lapse satisfies $\alpha(R) - 1 = (1 - 2M/R)^{1/2} - 1 \approx -1.9 \times 10^{-4}$ and $\langle v\rangle = 0$. The central core, i.e., the region within which the rest-mass density falls by no more than one-half its central value, is quite small: it is confined to the domain $0 \leq r_s/M \leq 7.7 \times 10^{-2}$ and contains only 0.48% of the total rest mass.

Consider next the black hole which forms from the catastrophic collapse of this extreme core-halo configuration. We are only able to follow the collapse numerically for a coordinate time amounting to 19 initial *central* free-fall time scales ($= 19[\langle\rho\rangle/\rho_c]^{1/2} = 1.2 \times 10^{-5}$ *mean* free-fall time scales). Beyond this point, the computation time required to follow particle orbits accurately near the high-density center, where the dynamical time scale is *very* small, becomes excessive, so we are forced to terminate our integrations. Nevertheless, already by this time, the black hole (as measured, say, by the apparent horizon) encompasses 3.1% of the total rest mass—over 6 times the mass of the initial central core—and is clearly still growing! Apparently, *even in the case of extremely centrally condensed configurations with extensive Newtonian halos, an appreciable fraction of the total mass collapses to a central black hole in a few dynamical times, provided the central redshift is sufficiently relativistic.*

A similar fate ensues in the collapse of the one other unstable $n = 4$ polytropic configuration whose evolution we follow on the computer. This configuration, with $z_c = 0.73$, is even more extreme (cf. Table 3), and yet, by the time our integrations terminate for this case, roughly 4.4% of its total rest mass—almost 7 times the core mass—already lies inside the apparent horizon.

An examination of the particle radial velocity profiles just outside the horizon reveals that *in both numerical examples the black holes are still growing at the end of our integrations.* Consider, in addition, the outermost particles at $t = 0$: they are at apocenter at the surface $r_s = R$. In any isotropic cluster, these "surface" particles have zero velocity at apocenter and orbit in radial trajectories. None of them have moved very far by the time our integrations terminate, but eventually they will penetrate the very center of the cluster. There they will be captured by the nascent black hole and thus add to its growing mass. Furthermore, once captured, these "surface" particles can never return to large radii; hence the mass interior to those particles orbiting just inside the surface at apocenter undergoes a net increase over its initial equilibrium value. Accordingly, some of these "near-surface" particles, which because of their slightly nonradial motion may have just barely escaped capture on their first passage through the center, are now much more likely to be captured on their second passage. An so forth for particles of successively smaller apocenter distances. The critical angular momentum per unit mass for capture ($l = 4M$ for test particles approaching from large distances with nonrelativistic velocities onto a static Schwarzschild black hole of mass M) clearly *increases* with time, making it more and more likely for particles with eccentric but not strictly radial orbits to be captured by the black hole once they penetrate the central regions.

The entire sequence of events described above inevitably leads to what Zel'dovich and Podurets (1965) surmised would be "an avalanche-type catastrophic contraction of the system" to a black hole. The whole process is over in just a few (mean) dynamical time scales. That Zel'dovich and his colleagues understood the significant qualitative features of collisionless, catastrophic collapse 20 yr ago without the aid of our simulations is attested to by their own remarkably detailed description of the process (1965, pp. 747, 748):

> In the problem of the motion of particles in a self-consistent field, the collapse of the orbits of some particles will lead to an increase of the field acting on the other particles, whose orbits will collapse in turn, etc. Thus, there will be an avalanche-type catastrophic contraction of the system once it has reached the critical state.
>
> Near the critical state, the contraction develops . . . with a characteristic time τ_k of the same order of magnitude as the time taken for a particle to complete one revolution.
>
> . . . The collapse of a system of particles is very complicated. The problem is more difficult than the nonstationary hydrodynamical problem, since in the problem concerning particles the state of matter at each point is determined not by several quantities (density, pressure, temperature, velocity), but by a function of the momentum vector.
>
> In the almost equilibrium state, a good approximation would be to consider the function isotropic, i.e., depending only on the magnitude and not on the direction of the momentum vector or, in other words, depending only on the energy.
>
> In the catastrophic-collapse problem, the situation is decidedly nonisotropic. Interesting qualitative features can be expected to make their appearance. There is a rapid contraction of the major portion of the mass.
>
> On the other hand, particles which in the initial almost-equilibrium state were moving near the outer boundary of the system in orbits close to circular ones will not be drawn into this contraction. After the contraction, these particles will create a cloud surrounding the main mass. The main mass will rapidly contract to its gravitational radius . . . . The particles in the cloud, following the laws of slow evolution, will only gradually fall into the collapsed mass.
>
> It is very desirable to perform calculations for such a model.

Elaborating several years later, Zel'dovich and Novikov (1971, p. 431) wrote:

> The physical picture of the collapse in this case is an increase of the core mass, accompanied by a transformation of formerly stable orbits into inward spirals, which lead the

core and accompanying stars into their collective gravitational radius. The noncircular orbits are important in this process because they connect the different layers of the cluster. A numerical investigation of such collapse is badly needed, but no one up to now has had the fortitude to attempt it.[2]

Verification of the "avalanche process" is implicit in the outcomes of all of our numerical integrations of collisionless, catastrophic collapse to a black hole. This cascading instability operates throughout the cluster, from the central core to the outer surface. *It is the "avalanche process" which ultimately allows a significant fraction of the total cluster mass to form a black hole, even when the initial central core, while relativistic, is but a small fraction of the total mass.*

The significance of this conclusion for relativistic star clusters likely to form in nature is detailed in Paper III. There it is argued that the central cores of dense, but otherwise Newtonian, clusters of neutron stars or stellar-mass black holes can evolve by the "gravothermal catastrophe" to a relativistic state in a Hubble time scale, provided the clusters are sufficiently massive and compact. Such clusters of compact stars may arise as the end products of advanced evolution in galactic nuclei. They will invariably be of the extreme core-halo type when they reach this relativistic state. Once their central redshifts become sufficiently large ($z_c \gtrsim 0.5$), they undergo catastrophic collapse to a black hole on a dynamical time scale. We have shown in this section that following collapse, the mass of the black hole formed at the center can be an appreciable fraction of the total mass of the initial cluster.

iii) *Power-Law Distribution with* $\delta = 3/2$

Equilibrium models were constructed and their evolutions were tracked on the computer for power-law distributions satisfying equation (9) with $\delta = 3/2$. This distribution was examined because the equilibrium models it generates near the first binding-energy maximum, while centrally condensed, are not so centrally condensed as in the previous example of an $n = 4$ polytrope (where $\delta = 5/2$). As a result, we are able to follow their nonlinear evolution much further before our integrations terminate.

The fractional binding energy versus central redshift curve for this equilibrium sequence is plotted in Figure 12. This figure again indicates the dynamical fates of selected models which we chose to evolve along the sequence with our simulation code. Additional features of these models are summarized in Table 4.

Figure 12 resolutely reconfirms our conclusion that the first binding-energy maximum locates the transition point between stability and instability in suitable one-parameter equilibrium sequences.

Quite interesting is the catastrophic collapse of the unstable model with $z_c = 0.65$ lying just beyond the binding-energy maximum. It is a centrally condensed configuration with $\langle \rho \rangle / \rho_c = 1.5 \times 10^{-3}$. Its core is highly relativistic, with $\alpha_c = 0.61$ and $\langle v \rangle = 0.54$. Even the halo, however, is somewhat relativistic, as the surface extends out no further than $R/M = 25$. By mass, the central core contains just 13% of the total rest mass and subtends the small region $0 \leq r_s/M \leq 1.6$.

A spacetime diagram for the collapse is shown in Figure 13. A blowup of this diagram showing the late stages of collapse is shown in Figure 14. We follow the collapse for only 28 initial central free-fall time scales or 1.1 mean free-fall time scales. By this time, a full 77% of the total rest mass, which amounts to 6 times the central core mass, has collapsed inside the trapped surface of the black hole which forms at the cluster center (see Fig. 14). An examination of the velocity profile (i.e., $\langle dr/dt \rangle = \langle u^r/u^0 \rangle$, where u^α is the velocity 4-vector and the angle brackets denote an average over many particles) at the end of our integration indicates that a substantial fraction of the remaining mass will also fall into the black hole.

The lapse profile during this collapse is shown in Figure 15 at various times. The "collapse of the lapse" is clearly evident at late times. The rest-mass density profile is plotted in Figure

[2] As should be obvious to the reader, we are only too pleased to be able to report here the results of the detailed numerical calculations desired—but already well anticipated—by Zel'dovich and his colleagues so many years ago. For a discussion of the "aftermath" of catastrophic collapse—i.e., the effects of a massive black hole residing at the center of a cluster of residual stars—see Shapiro (1985) and references therein.

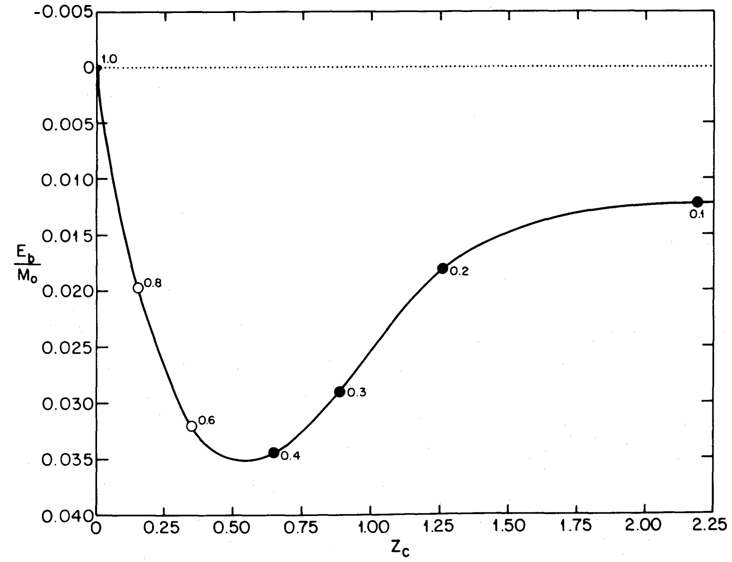

FIG. 12.—Power-law equilibrium sequence. The fractional binding energy E_b/M_0 is plotted as a function of central redshift z_c. Clusters along the sequence are labeled by their value of y_c (see Table 4). The dynamical fates of six models along the sequence are coded as in Fig. 1.

TABLE 4

POWER-LAW EQUILIBRIUM SEQUENCE[a]

y_c[b]	z_c	E_b/M_0	R/M	$\langle\rho\rangle/\rho_c$	Dynamical Fate
0.8......	0.147	0.0193	39.8	1.22×10^{-2}	Stable equilibrium
0.6......	0.347	0.0321	24.8	6.19×10^{-3}	Stable equilibrium
0.4......	0.649	0.0344	24.9	1.52×10^{-3}	Collapse to black hole
0.3......	0.884	0.0291	33.1	3.26×10^{-4}	Collapse to black hole
0.2......	1.26	0.0179	82.5	7.38×10^{-6}	Collapse to black hole
0.1......	2.19	0.0122	123	1.28×10^{-7}	Collapse to black hole

[a] $f(E) = K[(E/E_{\max})^2]^{-\delta}[1 - (E/E_{\max})^2]^\delta$ for $E \le E_{\max}$, $f = 0$ for $E > E_{\max}$, where K is a constant and $\delta = 3/2$.

[b] Relativity parameter y_c uniquely specifies a member of the sequence.

16. This figure also reveals that in spite of initial central concentration, most of the mass ends up inside the black hole following the unstable "avalanche" toward the center.

A more impressive realization of the avalanche effect occurs during the collapse of the most extreme core-halo configuration considered in this sequence, i.e., the unstable model with $z_c = 2.2$ in Table 4 and Figure 12. This extreme configuration is very centrally condensed, with $\langle\rho\rangle/\rho_c = 1.3 \times 10^{-7}$, and very relativistic near the center, with $\alpha_c = 0.31$ and $\langle v \rangle = 0.75$. The central core contains only 1.9% of the total rest mass. The remaining halo extends far out into the Newtonian regime, as the surface reaches to $R/M = 123$. We can track this collapse for only 25 central or 0.9×10^{-2} mean initial free-fall time scales. Nevertheless, by the time the integrations terminate, a full 16% of the total rest mass (8 times the mass of the central core!) has collapsed inside the trapped surface. This outcome supports our conclusion that an appreciable fraction of an unstable cluster can collapse to a black hole even when the cluster is extremely centrally concentrated and possesses an extensive Newtonian halo.

iv) *Newtonian Polytropes: Stability versus Instability*

Consider equation (9) in the Newtonian limit, when $1 - E_{\max}/\mu_0 \ll 1$ and $(E_{\max} - E)/\mu_0 \ll 1$. In this regime, the distribution function reduces to

$$f(E) \approx \begin{cases} K'(E_{\max} - E)^\delta , & E \le E_{\max} , \\ 0 , & E > E_{\max} , \end{cases} \tag{10}$$

where the new normalization constant K' is related to the old constant K via $K' = (2/\mu_0)^\delta K$. It is well known that spherical equilibrium configurations obeying equation (10) correspond to collisionless polytropes with index $n = \delta + 3/2$ and $\Gamma \equiv (d \ln P)/(d \ln \rho_0) = (2\delta + 5)/(2\delta + 3)$ (see Zel'dovich and Novikov 1971 for an excellent review and references). The allowed values of δ (to ensure that the integrals for ρ_0 and P are finite) for equilibrium are

$$-1 < \delta < \infty \quad \text{(for equilibrium)} \tag{11}$$

corresponding to

$$\tfrac{1}{2} < n < \infty \quad \text{(for equilibrium)} . \tag{12}$$

Curiously, the stability of collisionless, spherical polytropes

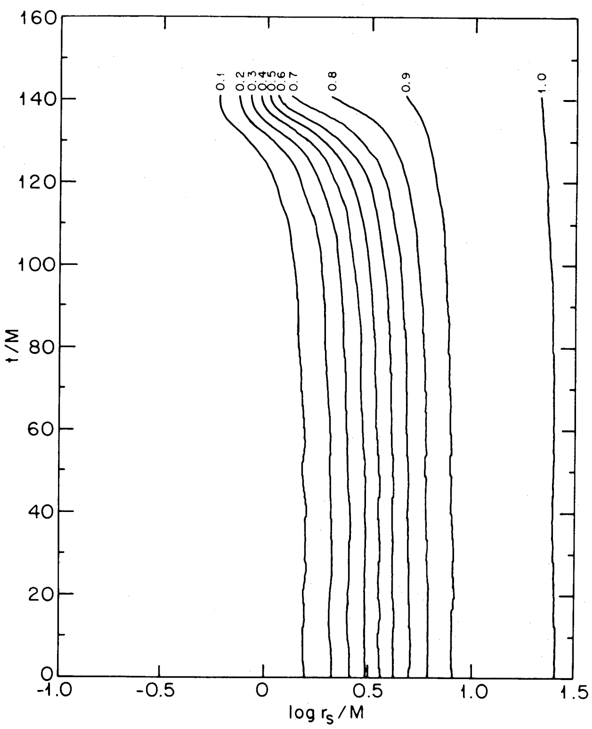

FIG. 13

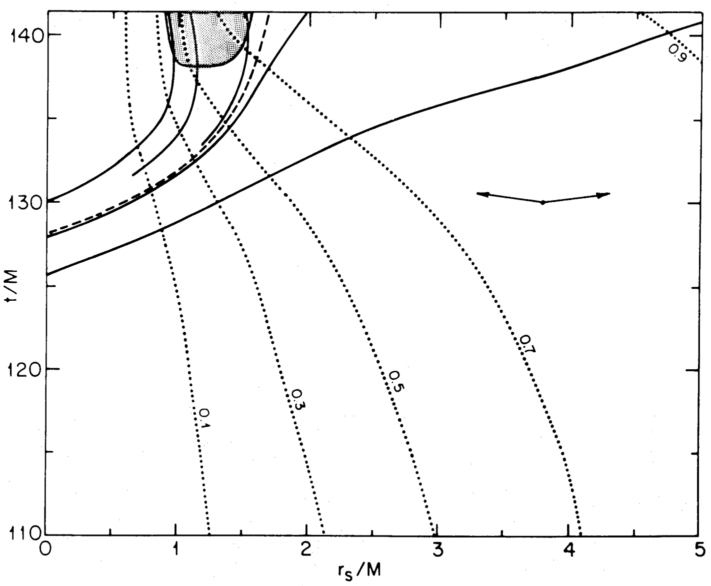

FIG. 14

FIG. 13.—Spacetime diagram for the power-law cluster initially in equilibrium with $y_c = 0.4$. The solid lines are the world lines of imaginary Lagrangian matter tracers labeled by their fixed interior rest-mass fraction. The configuration collapses to a black hole.

FIG. 14.—Blowup of Fig. 13 at late times. Diagram is labeled as in Fig. 3.

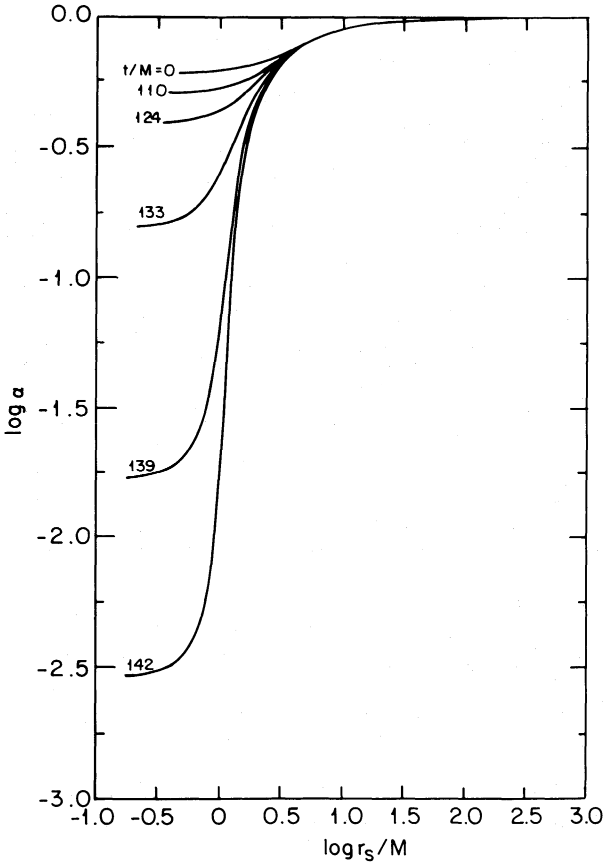

FIG. 15.—The lapse function α as a function of areal radius r_s on selected time slices for the power-law cluster shown in Fig. 13.

to radial perturbations is known for only a limited range of δ. For example, it follows from Antonov (1960, 1962) that all polytropic bounded models with monotonically decreasing distribution functions $f'(E) < 0$ are stable, i.e., polytropes with $0 < \delta < 7/2$ $(3/2 < n < 5)$ are stable. [Antonov 1962 and Lynden-Bell and Sanitt 1969 have also shown that all the *non-spherical* modes are stable whenever $f'(E) < 0$.] Lynden-Bell and Sanitt (1969) proved that an equilibrium configuration satisfying $f'(E) < 0$ is stable if the corresponding fluid sphere is stable. Applied to polytropes, their theorem proves the stability of configurations with $0 < \delta < 3/2$ $(3/2 < n < 3)$, in accord with Antonov's more powerful result. Stronger still is the general claim of Sygnet *et al.* (1984), who prove that *all* collisionless spherical equilibria with $f'(E) < 0$ are stable (see also Gillon, Doremus, and Baumann 1976; Kandrup and Sygnet 1985). This result would guarantee that all polytropes with $\delta > 0$ are stable.

As noted by Zel'dovich and Novikov (1971), all the applicable stability theorems require that $\partial f/\partial E < 0$. There is no proof that violation of this criterion necessary implies instability, although these authors speculate that "it is very probable that this is the case." In particular, they suggest that "polytropic solutions with $\delta < 0$ $(n < 3/2)$ are probably unstable" (but see footnote 1 above).

In the absence of rigorous theorems, the dynamical stability of polytropes in the allowed range $-1 < \delta < 0$ $(1/2 < n < 3/2)$ is a problem ripe for numerical investigation. A numerical study of this question was first performed by Henon (1973; see also Barnes, Goodman, and Hut 1985), who employed a Newtonian, concentric shell simulation code with phase space symmetries identical to our own. He found, surprisingly, that all polytropic models are dynamically stable almost down to the $n = 1/2$ limiting case. In the case $n = 1/2$ $(\delta = -1)$, collective oscillations of the configurations, which were absent in other cases with $n > 1/2$, are noticeable and slowly growing. Thus, this case appears to be slightly unstable, although numerical noise makes it difficult to decide whether or not the oscillations are truly unstable. Henon estimates the boundary between stable and unstable configurations to be $n = 0.5$–0.6. However, he does not exclude the possibility that the critical value is actually $n = 1/2$, to that all polytropic models with $f = f(E)$ are in fact stable.

In light of the significance of Henon's findings, we have reinvestigated this intriguing issue. Specifically, we have employed our own code to track the dynamical evolution of Newtonian polytropes described by equation (10) in the interesting regime $-1 < \delta < 0$ $(1/2 < n < 3/2)$. Spacetime diagrams for three cases are shown in Figure 17. The initial equilibrium configurations in Figures 17*a*, 17*b*, and 17*c* have power-law exponents $\delta = -0.5$, -0.75, and -0.99 and initial radii $R/M = 2.0 \times 10^4$, 1.7×10^4, and 1.5×10^4 respectively. Since these configurations are described by Newtonian, power-law profiles, the results for the dynamical behavior of *any* model with

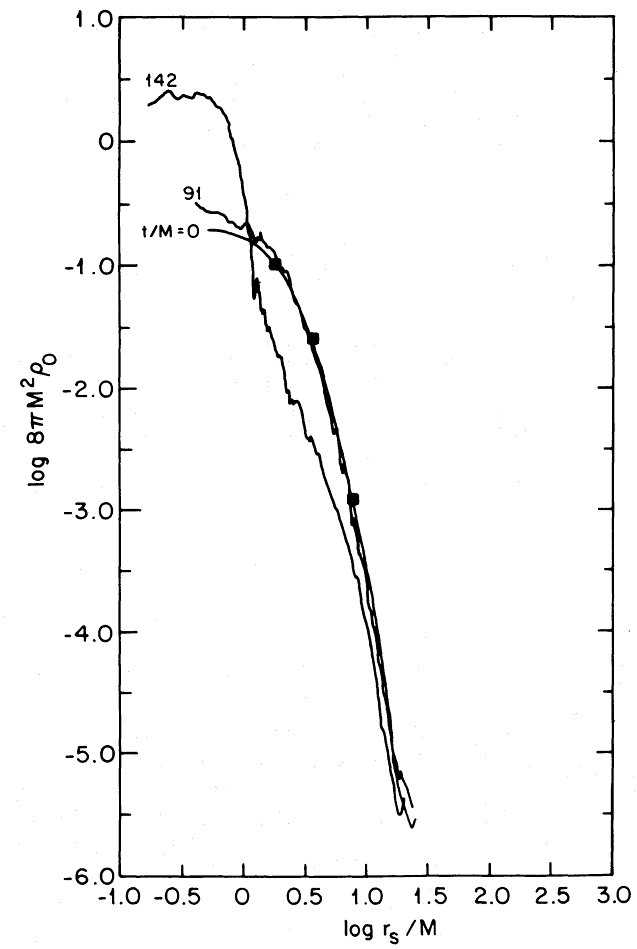

FIG. 16.—The rest-mass density ρ_0 as measured by a normal observer for the case described in Fig. 15. The boxes indicate the 10%, 50%, and 90% interior rest-mass points at $t = 0$. They reveal the high degree of central concentration.

the same exponent δ is identical (up to appropriate scale factors) to the behavior of the particular case illustrated here.

To within the numerical accuracy of the calculations, our results confirm the findings of Henon (1973) regarding the stability of collisionless, spherical polytropes with $f'(E) > 0$. For the most part, the oscillations in Figure 17 represent stable, low-amplitude noise induced by the discrete nature of the initial data. In this respect they closely resemble the plotted results of Henon. There is some suggestion in Figure 17c that the case $\delta = -0.99$ ($n = 0.51$) exhibits unstable growing oscillations near the surface. The same feature is apparent in the case $\delta = -0.75$ ($n = 0.75$), although to a lesser extent. However, closer examination of the output shows that in both cases it is essentially only a *single* particle which is responsible for the outward drift of the surface. Moreover, energy conservation begins to break down at the $\lesssim 10\%$ level toward the end of our integration for the $\delta = -0.99$ case. Noting that these computations only utilized the modest set of "standard" integration accuracy parameters described earlier, we tentatively attribute apparent small deviations from completely stable equilibrium behavior at late time to numerical inaccuracies. *Newtonian polytropes are thus stable, almost to and perhaps including the limiting case* $\delta = -1, n = 0.5$.

III. VIOLENT RELAXATION IN GENERAL RELATIVITY

a) *Qualitative Overview*

Consider any stable member of a collisionless, spherical equilibrium sequence. For simplicity, assume that the chosen configuration is Newtonian. Define a nondimensional internal energy ("temperature") parameter ϵ according to

$$\epsilon \equiv 2E_K/|W| , \tag{13}$$

where E_K is the internal kinetic energy and W is the total Newtonian gravitational potential energy. By the virial theorem, we must have

$$\epsilon = 1 \quad \text{(equilibrium: no collapse)} \tag{14}$$

for this static equilibrium configuration. Now imagine an identical configuration, with the same density profile as the first, but with zero kinetic energy, i.e., with all particles completely motionless. For this cold, momentarily static configuration we have

$$\epsilon = 0 \quad \text{(nonequilibrium: collapse to a black hole).} \tag{15}$$

Such a dust sphere will immediately undergo catastrophic (Bondi-Tolman) collapse to a Schwarzschild black hole on a dynamical free-fall time scale. (For a numerical demonstration in the trivial case of a homegeneous dust ball, i.e., Oppenheimer-Synder collapse, see Paper I, § VIIa.)

An intriguing issue here concerns the fate of momentarily static, bound configurations with *intermediate* values of ϵ between 0 and 1. Clearly, for any $\epsilon < 1$, the configuration is not sufficiently "hot" to be in viral equilibrium and hence will begin to collapse the instant it is released. Now if ϵ is sufficiently small, the angular momentum of a typical particle will be small enough that, at pericenter, the particle will be inside the Schwarzschild radius of the collapsing configuration. In this case the collapse will continue to completion, resulting in the formation of a central black hole. Alternatively, if ϵ is sufficiently large, the angular momentum of typical particles will be large enough to avoid this catastrophic fate. In this situation particles can safely pass pericenter and head back out to large radii without forming an event horizon. The collapse will effectively be reversed by a collective particle "bounce" at pericenter. As the particles in the very center following turnaround stream back out into the ambient cluster, they encounter a counterstream of ingoing particles which have yet to reach pericenter. Such counterstreaming leads to the well-known collisionless, two-stream instability followed by Landau damping. In this situation, collective fluctuations in the gravitational potential field lead to particle thermalization. In the context of stellar dynamics, this effect is known as "violent relaxation" or "dynamical phase mixing" and was first described in detail by Lynden-Bell (1967). Hence, *if ϵ is large enough, the initial collapse will be reversed, and violent relaxation will drive the system to virial equilibrium in a few dynamical periods.*

In a very real sense, then, a self-gravitating, momentarily static, bound configuration can experience a gravitational "phase change" to a singular state, depending upon the value of $0 < \epsilon < 1$. There is thus a critical value of $\epsilon = \epsilon_{\rm crit}$ such that

$$\begin{aligned} \epsilon > \epsilon_{\rm crit} &\Rightarrow \text{collapse} \rightarrow \text{bounce} \\ &\qquad \rightarrow \text{violent relaxation} \rightarrow \text{virialization} , \\ \epsilon < \epsilon_{\rm crit} &\Rightarrow \text{catastrophic collapse to a black hole} . \end{aligned} \tag{16}$$

It is general relativity and the possibility of black holes that makes this "critical phenomenon" possible. Note that the distinction between the two final states is quite sharp. Specifically, for all $\epsilon < \epsilon_{\rm crit}$, the final radius of the configuration is $R_f \approx 2M$, the Schwarzschild radius. However, for any $1 > \epsilon > \epsilon_{\rm crit}$, the characteristic radius of the final virialized cluster R_f is quite comparable to the characteristic radius of the initial configuration R by energy conservation. Thus, even if the initial configuration is quite "cold" ($1 \gg \epsilon > \epsilon_{\rm crit}$), energy conservation demands

$$E = E_K + W \approx W_i \approx W/2 , \tag{17}$$

where the virial theorem has been used in the last equality. Ignoring coefficients of order unity that depend on the initial and final particle distributions, we have $|W| \approx M^2/R$, whereby equation (17) yields

$$R_f \approx R/2 . \tag{18}$$

If the initial configuration is not so cold ($1 \approx \epsilon > \epsilon_{\rm crit}$), the initial and final radii will be even closer.

We can estimate $\epsilon_{\rm crit}$ trivially for a typical sperical configuration of mass M, radius R by focusing on a "characteristic" star and demanding that it just graze $r_s = 2M$ at pericenter. Ignoring numerical factors of order unity, we may employ angular momentum conservation to write

$$\tilde{l}_{\rm crit} \approx v_{\rm crit} R \approx M , \tag{19}$$

where $\tilde{l}$ is the typical angular momentum per unit mass and $v_{\rm crit}$ is the typical internal velocity in the critical configuration. Equations (13) and (19) thus imply

$$\epsilon_{\rm crit} \approx \frac{v_{\rm crit}}{c} \approx \frac{GM}{Rc^2} , \tag{20}$$

where we have temporarily restored Gs and cs. Note that in Newtonian dynamics, where $c \rightarrow \infty$, we have $\epsilon_{\rm crit} \rightarrow 0$, so the possibility of a "phase transition" effectively disappears. For this reason, *Newtonian N-body codes can never reveal such behavior.*

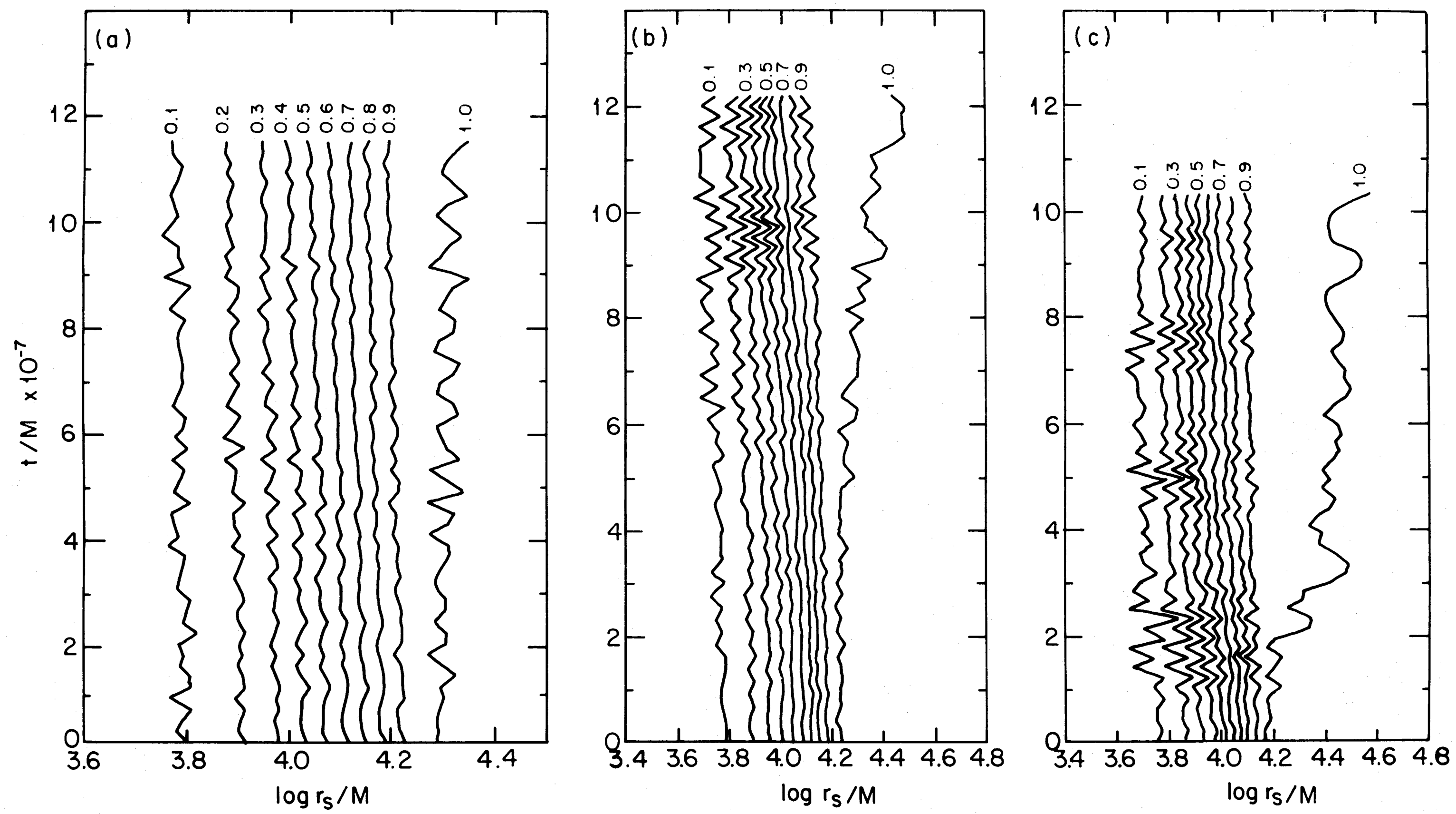

FIG. 17.—Spacetime diagrams of Newtonian polytropic clusters initially in equilibrium. The solid lines are the world lines of Lagrangian matter tracers labeled by their fixed interior rest-mass fraction. Models *a*, *b*, and *c* have power-law exponents $\delta = -0.5$ ($n = 1$), $\delta = -0.75$ ($n = 0.75$), and $\delta = -0.99$ ($n = 0.51$) respectively.

The above estimates can be made more rigorous in specific cases. For example, recall the spherical, momentarily static, homogeneous configurations consisting of particles in tangential orbits examined in Paper I, Appendix B. In the Newtonian limit ($M/R \ll 1$), these particles move with speed

$$v^{\phi}(r) = \xi V_{\rm cir}(r_s) = \xi \frac{r_s}{R}\left(\frac{M}{R}\right)^{1/2} , \quad 0 < \xi < 1 , \tag{21}$$

where ξ is a constant. In that Appendix, we showed that the critical condition for the collapse of the configuration to a black hole is

$$\xi < \xi_{\rm crit} \approx 4(M/R)^{1/2} . \tag{22}$$

Accordingly, at the surface $r_s = R$, equations (21) and (22) imply

$$v^{\phi}_{\rm crit}(R) = 4M/R , \tag{23}$$

which is consistent with the crude estimate given by equation (20).

b) *A Numerical Demonstration*

We have evolved on the computer several homogeneous, tangential-orbit clusters of the kind described in the previous paragraph. The case defined by $R/M = 10$, $\xi = 0$ corresponds to Oppenheimer-Synder dust collapse to a black hole and was already detailed in Paper I (see § VII*a*). We now consider the case $R/M = 100$, $\xi = 0.5$. According to equation (22), we have $\xi_{\rm crit} = 0.4$. While the "temperature" parameter chosen here is close to $\xi_{\rm crit}$, it nevertheless satisfies $\xi > \xi_{\rm crit}$. Hence, we anticipate that while the initial collapse may proceed to small radii, where the gravitational fields are quite relativistic, it will ultimately be reversed by a collective particle "bounce." We then expect that "violent relaxation" will operate to bring about virialization in a few dynamical times, as the configuration settles into a final equilibrium state.

Our numerical results for this example are summarized in Figures 18–21. In Figure 18 we plot a spacetime diagram showing selected Lagrangian world lines in the matter distribution. It is quite apparent from this figure that our expectations are realized. The initial collapse is indeed reversed and after a few oscillations, the configurations settles into a stable, nonsingular, equilibrium state. The final half-mass radius is at $r_s \approx 18$; 95% of the mass lies within $r_s/M \approx 30$. The Newtonian virial relation $E = W/2$ holds to within 14%, which, allowing for relativistic corrections, is quite reasonable. The relativistic energy parameter E_0 (cf. eq. [50] of Paper I), which is strictly conserved in a true equilibrium configuration, varies by no more than 1.4% during the entire final time interval $4.9 \times 10^3 \leq t/M \leq 22 \times 10^3$.

The rest-mass density profiles are plotted in Figure 19 at several times. Violent relaxation drives the initial homogeneous sphere (recall $\rho_0 \approx \rho$, since $R/M \gg 1$) to a final "central core, power-law halo" configuration. The central core contains most of the mass. The corresponding velocity dispersion profiles are plotted in Figure 20, and the isotropy of the velocity dispersions is examined in Figure 21. Violent relaxation clearly serves to "thermalize" somewhat the initial tangential, linear velocity profile given by equation (21). Shell crossing and phase mixing generate a radial component in the final velocity dispersion where there was none to begin with. Of course, our restriction to perfect spherical symmetry limits violent relaxation to thermalization in the *radial* direction only. Thermalization to a true relativistic Maxwell-Boltzmann state presumably requires transverse potential field fluctuations as well.

We remark, finally, that general relativity was crucial in allowing violent relaxation to operate in the example con-

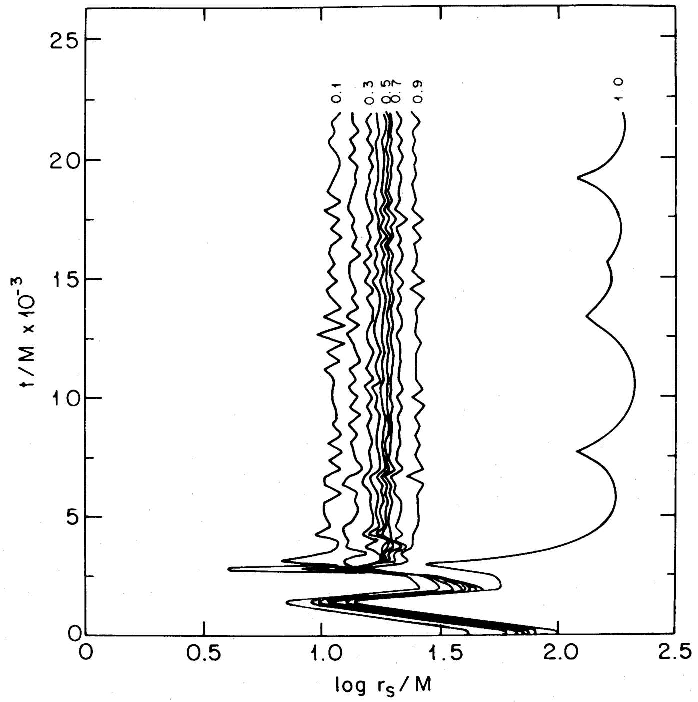

FIG. 18.—Spacetime diagram for relativistic violent relaxation. An initially homogeneous cluster with tangential orbits collapses from $R/M = 100$. After an initial implosion and oscillation phase, the configuration settles down to a quasi-static equilibrium.

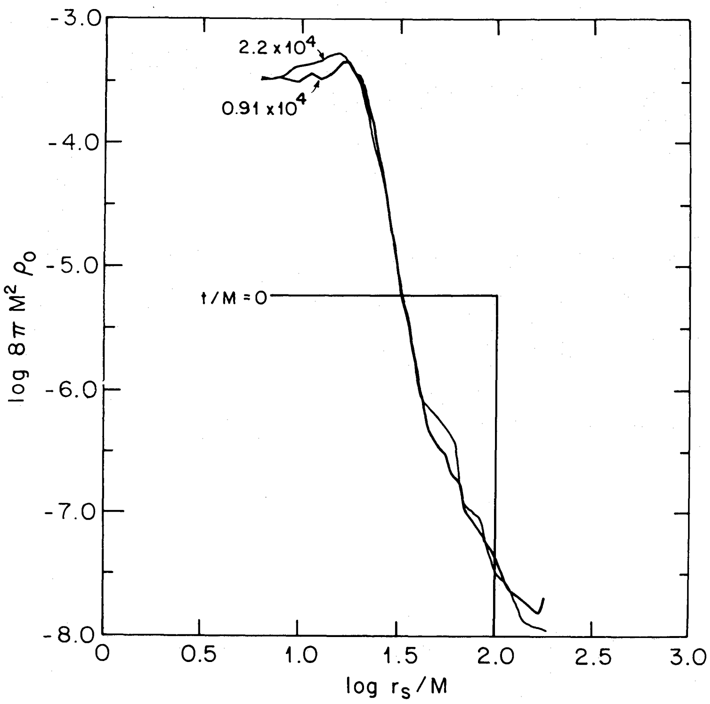

FIG. 19.—The rest-mass density ρ_0 for the case described in Fig. 18. From an initial homogeneous profile, the cluster develops a centrally condensed core-halo structure.

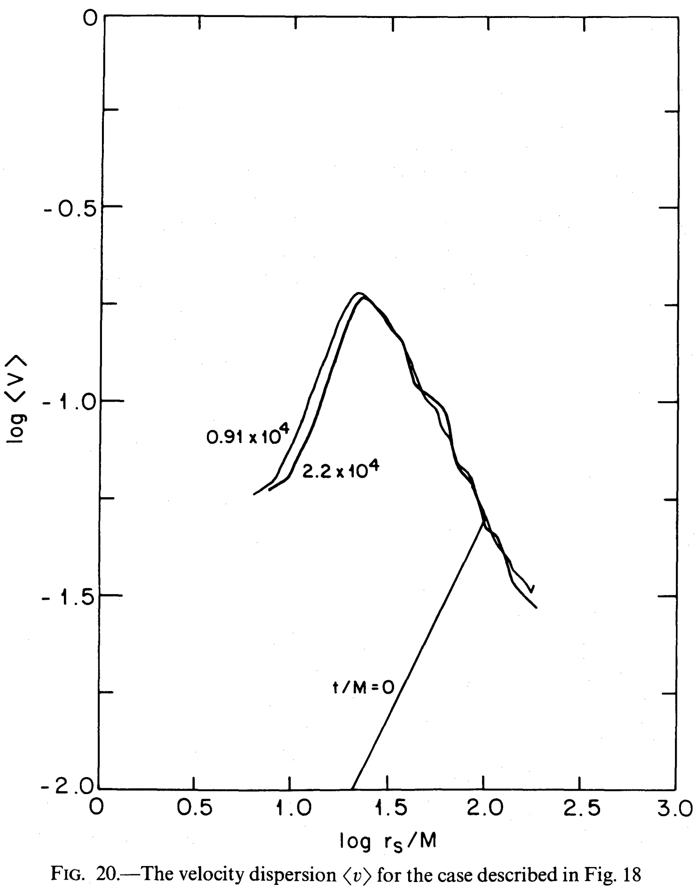

FIG. 20.—The velocity dispersion $\langle v \rangle$ for the case described in Fig. 18

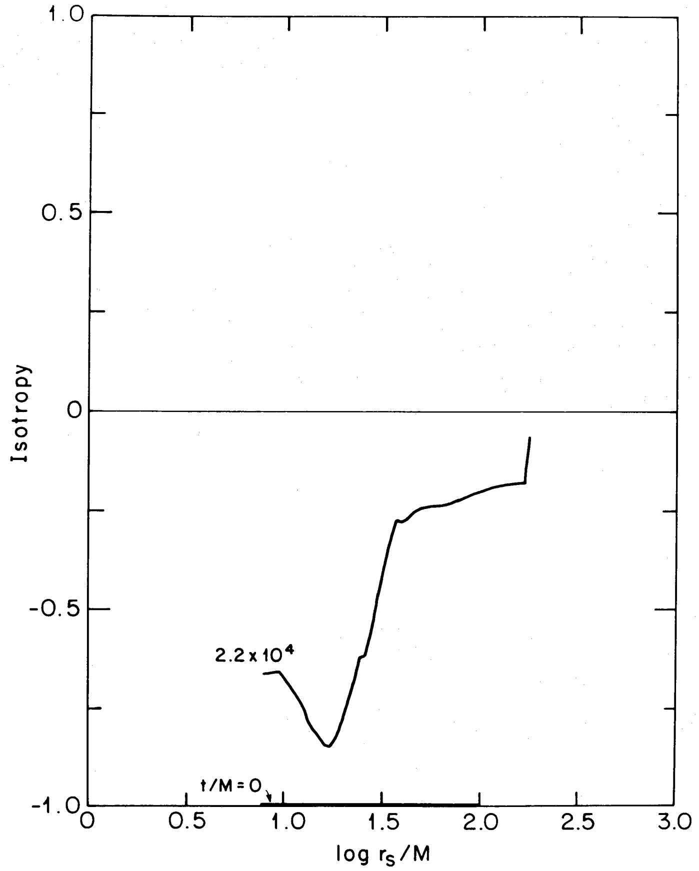

FIG. 21.—The isotropy measure for the case described in Fig. 18

sidered above. For *strictly* Newtonian gravity, a homogeneous, tangential-orbit sphere oscillates homologously forever, maintaining its homogeneous shape and linear velocity profile (see Appendix C of Paper I for an analysis). No shell crossing occurs. In general relativity, however, shell crossing does occur and takes place sooner for particles that penetrate deeper into the relativistic field domain. *It is shell crossing that permits violent relaxation or dynamical phase mixing to take place during spherical collapse.*

c) *Possible Astrophysical Implications*

The astrophysical significance of relativistic violent relaxation and the gravitational "critical point" phenomenon has yet to be explored. We speculate that it may have cosmological relevance for bound, collisionless clumps which may form in the early universe. For consider a bound, spherical primordial fluctuation that reaches maximum expansion and is on the verge of recollapse. If its subsequent evolution is described by collisionless particle dynamics, then its ultimate dynamical fate is sealed by its phase space distribution at this moment of maximum expansion. Specifically, if it is sufficiently "cold," i.e., if its random internal energy is small so that $\epsilon < \epsilon_{\rm crit}$, then the perturbation will collapse to form a black hole. Otherwise, if $\epsilon > \epsilon_{\rm crit}$, its collapse will be reversed and violent relaxation will drive it to an equilibrium final state. One key question is: *Do there exist collisionless particles with nonzero rest mass whose properties make them good candidates for forming bound, cold* ($\epsilon < \epsilon_{\rm crit}$) *clumps in the early universe?* If there are such particles, then *the black holes they form may provide convenient sites for hiding dark matter and missing mass.* We fell that this issue warrants further study.

This work has been supported by National Science Foundation grants AST 84-15162 and PHY 83-05288.

REFERENCES

Antonov, V. A. 1960, *Astr. Zh.*, **37**, 918 [English trans. in *Soviet Astr.—AJ*, **4**, 859 (1961)].
———. 1962, *Vestn. Leningr. Gos. Univ.*, No. 19, p. 96.
Barnes, J., Goodman, J., and Hut, P. 1985, preprint.
Eardley, D. M., and Smarr, L. 1979, *Phys. Rev. D*, **19**, 2239.
Fackerell, E. D. 1966, Ph.D. thesis, University of Sydney.
———. 1970, *Ap. J.*, **160**, 859.
Gillon, D., Doremus, J. P., and Baumann, G. 1976, *Astr. Ap.*, **48**, 467.
Goodman, J., and Hut, P. 1985, ed., *IAU Symposium 113, Dynamics of Star Clusters* (Dordrecht: Reidel).
Hawking, S. W., and Ellis, G. F. R. 1973, *The Large Scale Structure of Space-Time* (Cambridge: Cambridge University Press).
Henon, M. 1973, *Astr. Ap.*, **24**, 229.
Ipser, J. R. 1969, *Ap. J.*, **158**, 17,
———. 1980, *Ap. J.*, **238**, 1101.
Ipser, J. R., and Thorne, K. S. 1968, *Ap. J.*, **154**, 251.
Kandrup, H. E., and Sygnet, J. F. 1985, *Ap. J.*, **298**, 27.
Katz, J., Horwitz, G., and Klapisch, M. 1975, *Ap. J.*, **199**, 307.
Lightman, A. P., and Shapiro, S. L. 1978, *Rev. Mod. Phys.*, **50**, 437.
Lynden-Bell, D. 1967, *M.N.R.A.S.*, **136**, 101.

Lynden-Bell, D., and Sanitt, N. 1969, *M.N.R.A.S.*, **143**, 167.
Misner, C. W., Thorne, K. S., and Wheeler, J. A. 1973, *Gravitation* (San Francisco: Freeman) (MTW).
Petrich, L., Shapiro, S. L., and Teukolsky, S. A. 1985, *Phys. Rev. D*, **31**, 2459 (PST).
Shapiro, S. L. 1985, in *IAU Symposium 113, Dynamics of Star Clusters*, ed. J. Goodman and P. Hut (Dordrecht: Reidel), p. 373.
Shapiro, S. L., and Teukolsky, S. A. 1985*a*, *Ap. J.*, **298**, 34 (Paper I).
———. 1985*b*, *Ap. J.* (*Letters*), **292**, L41 (Paper III).
Smarr, L., and York, J. W. 1978, *Phys. Rev. D*, **17**, 2529.
Sobouti, Y. 1984, *Astr. Ap.*, **140**, 82.
Spitzer, L. 1975, in *IAU Symposium 69, Dynamics of Stellar Systems*, ed. A. Hayli (Dordrecht: Reidel), p. 3.
———. 1985, in *IAU Symposium 113, Dynamics of Star Clusters*, ed. J. Goodman and P. Hut (Dordrecht: Reidel), p. 109.
Suffern, K. G., and Fackerell, E. D. 1976, *Ap. J.*, **203**, 477.
Sygnet, J. F., Des Forêts, G., Lachièze-Rey, M., and Pellat, R. 1984, *Ap. J.*, **276**, 737.
Zel'dovich, Ya. B., and Novikov, I. D. 1971, *Relativistic Astrophysics*, Vol. **1** (Chicago: University of Chicago Press).
Zel'dovich, Ya. B., and Podurets, M. A. 1965, *Astr. Zh.*, **42**, 963 [English trans. in *Soviet Astr.—AJ*, **9**, 742 (1966)].

STUART L. SHAPIRO and SAUL A. TEUKOLSKY: Space Sciences Bldg., Cornell University, Ithaca, NY 14853